

Signal from Structure: Exploiting Submodular Upper Bounds in Generative Flow Networks

Alexandre Larouche^{1,2} Audrey Durand^{1,2,3}

Abstract

Generative Flow Networks (GFlowNets; GFNs) are a class of generative models that learn to sample compositional objects proportionally to their a priori unknown value, their reward. We focus on the case where the reward has a specified, actionable structure, namely that it is submodular. We show submodularity can be harnessed to retrieve upper bounds on the reward of compositional objects that have not yet been observed. We provide in-depth analyses of the probability of such bounds occurring, as well as how many unobserved compositional objects can be covered by a bound. Following the Optimism in the Face of Uncertainty principle, we then introduce SUBO-GFN, which uses the submodular upper bounds to train a GFN. We show that SUBO-GFN generates *orders of magnitude* more training data than classical GFNs for the same number of queries to the reward function. We demonstrate the effectiveness of SUBO-GFN in terms of distribution matching and high-quality candidate generation on synthetic and real-world submodular tasks.

1. Introduction

Sampling from hard-to-approximate distributions has been a long-studied problem (Metropolis et al., 1953). Some difficulties are aggravated when sampling objects from large combinatorial spaces, e.g. in drug discovery (Shen et al., 2023b) and protein design (Jain et al., 2022), namely the generation of said objects. Fortunately, many problems allow for the objects to be composed through a sequence of steps, resulting in compositional objects. In the specific setting where one aims to sample compositional objects proportionally to their unknown *value* (the reward), Generative Flow Networks (GFlowNets, or GFNs) (Bengio et al., 2021;

¹Département d'informatique et de génie logiciel, Université Laval, Québec, Canada ²Mila - Quebec AI Institute, Montréal, Canada ³Canada CIFAR AI Chair. Correspondence to: Alexandre Larouche <allar145@ulaval.ca>.

2023) were recently introduced as a framework to approximate the target sampling distribution through sequential, episodic learning.

The success of GFNs is partly driven by their ability to sample a diverse set of candidates in large combinatorial spaces (Zhang et al., 2023b; Bengio et al., 2021), paving the way for their application in many domains, such as molecule generation (Koziarski et al., 2024), sensor selection (Evmorfos et al., 2023), and scheduling (Zhang et al., 2022). A growing body of works study how GFNs can be improved by relying on properties of the compositional objects such as symmetry (Ma et al., 2023) and ordering (Chen & Mauch, 2023), or domain specific knowledge (Koziarski et al., 2024; Seo et al., 2024; Mistal et al., 2023). However, none focus on how the structure of the reward, the most elementary constituent of GFNs, can be exploited.

So far, GFNs have been primarily studied in problems with arbitrary reward structure (Zhang et al., 2023b; Koziarski et al., 2024; Zhang et al., 2022; Bengio et al., 2021). In this work, we consider reward functions that are submodular set functions. Submodularity encodes the *diminishing return* property, where adding an element to a small set must produce an increase in value no less than that of adding the element to one of its superset. This structure naturally occurs in many real-world problems, for example in genetics (Gasperini et al., 2019), sensor selection (Evmorfos et al., 2023; Shamaiah et al., 2010) and influence maximization (Domingos & Richardson, 2001; Zhang et al., 2025). We investigate how the submodular structure of the reward function can be leveraged by GFNs to improve their estimate of the target sampling distribution.

Contributions We first show that the submodularity of the reward function can be harnessed to retrieve upper bounds on the reward of compositional objects that have not yet been observed. We provide an in-depth theoretical analysis of the probability of obtaining such bounds, as well as how many unobserved objects can be covered by a bound. Following the *Optimism in Front of Uncertainty* (OFU) principle (Brafman & Tennenholz, 2002), we then introduce SUBO-GFN, an approach that uses the submodular upper bounds for training a GFN. We find that SUBO-GFN generally produces *orders of magnitude* more learning signals

per query to the reward function than regular GFNs. Furthermore, we theoretically investigate the impact of being optimistic (using upper bounds) on the learned distribution. Finally, we demonstrate the effectiveness of SUBO-GFN on synthetic and real-world submodular tasks, where we discuss its practical implications for both distribution matching and the generation of diverse high-quality candidates.

2. Related Works

Optimism in the Face of Uncertainty Our work relies on learning from upper bounds on the reward of unobserved objects (i.e. an optimistic estimate). As such, there is a deep connection with the *Optimism in the Face of Uncertainty* (OFU) principle, which states that when uncertain about the value of an object, one should assume the best case scenario. OFU is commonly used in bandits such as the Upper Confidence Bound (UCB) family of algorithms (Auer et al., 2002; Li et al., 2010; Zhou et al., 2020). This principle has been quite successful in dealing with the *exploration-exploitation tradeoff* that sequential decision making problems often face. UCB-style mechanisms are extensible to reinforcement learning (Auer & Ortner, 2006; Brafman & Tennenholz, 2002; Azar et al., 2017; Dann et al., 2017) and GFNs (Bengio et al., 2023; Jain et al., 2022). However, in the GFN literature, the impact of using upper bounds as a learning signal remains unstudied.

Improving GFN Exploration Many works have focused on improving the exploration mechanisms in GFNs. Some, such as Generative Augmented Flow Networks (Pan et al., 2022) and Sibling-Augmented GFNs (Madan et al., 2024) implement intrinsic motivation as an exploration mechanism. Local Search GFNs (Kim et al., 2023) instead integrate a local search heuristic that backtracks from generated objects to find nearby improvements to candidate solutions. Finally, Thompson Sampling has been studied as a mechanism to guide exploration in GFNs (Rector-Brooks et al., 2023). The approaches attempting to improve exploration should be seen as complementary to our work, as they are compatible. However, specifying a reward structure allows us to provide theoretical analyses which pave the way towards problem dependent data-efficiency and exploration mechanisms.

GFNs with Intermediate Learning Signal Traditional GFN settings typically assume that only the value of fully-defined compositional objects can be observed (Bengio et al., 2021; 2023). In this work, we consider a relaxed setting where the value of intermediate objects in-the-making can be observed as well. Such relaxed setting has been considered in Forward-Looking strategies for GFNs (Pan et al., 2023; Zhang et al., 2023b;a; Sendera et al., 2024), which use intermediate values to improve local credit assignment in an attempt to mitigate sparse and delayed learning signals.

Similarly, LED-GFNs (Jang et al., 2023) learn to decompose energy functions dependent on the reward to better assign credit. Crucially, these methods typically treat intermediate signals to improve learning in the current trajectory. They do not exploit the structural properties of these rewards (such as submodularity) to infer information about unobserved objects. In this work, we argue that intermediate learning signal in structured environments can be used not just for credit assignment, but as a source of (quasi-)free data augmentation for global exploration.

3. Problem Setting

We consider the problem of sampling compositional objects proportionally to their value. Formally, let $(\mathcal{S}, \mathcal{A})$ be a tuple describing a directed acyclic graph (DAG), where \mathcal{S} is called the state-space and \mathcal{A} is called the action-space. A compositional object is built by sequentially selecting elements from \mathcal{A} . A state $s \in \mathcal{S}$ denotes the set of elements describing an object, and an action $a \in \mathcal{A}$ corresponds to the addition of element a to s . We assume $|\mathcal{A}| = N$ and denote $\mathcal{A}(s) := \mathcal{A} \setminus s$ the elements that are not yet contained in the state s . The action $a \in \mathcal{A}(s)$ causes a transition from state s to the new state $s' = s \cup \{a\}$, denoted $s \rightarrow s'$. Let $\mathcal{X} := \{s \in \mathcal{S} : |s| = C\}$ be a special subset of \mathcal{S} called the *terminating state-space*, where $C \in \mathbb{N}_{>0}$ is a cardinality constraint. A *trajectory* corresponds to a sequence of states obtained by sequentially adding elements to the *initial state* $s_0 := \emptyset$ until the cardinality constraint C is met, that is until a terminating state $x \in \mathcal{X}$ is encountered. We use \mathcal{T} to denote the set of all possible trajectories.

The *reward* function $R : \mathcal{S} \mapsto \mathbb{R}_{>0}$ assigns a value to each state. The objective is to sample trajectories ending in $x \in \mathcal{X}$ with probability $R(x)/Z$, where $Z = \sum_{x \in \mathcal{X}} R(x)$ is the *partition function*. We focus on the setting where the reward function R is a submodular set function.

Assumption 3.1 (Submodular reward function). The reward function R is submodular if $R(s \cup \{a\}) - R(s) \geq R(s' \cup \{a\}) - R(s')$ for any states $s, s' \in \mathcal{S}$ such that $s \subset s'$, and action $a \in \mathcal{A}(s')$.

Submodularity models diminishing returns (i.e., adding an element a to s must produce an increase in value no less than that of adding element a to $s' \supseteq s$). Figure 1 illustrates an example of a DAG with a submodular constraint on the reward function. A lot of information about the problem can be inferred by observing the reward of a few states in \mathcal{S} .

3.1. Generative Flow Networks

Generative Flow Networks (GFNs, Bengio et al. (2021; 2023)) are a class of methods for sampling compositional objects proportionally to their reward. GFNs learn to distribute the *flow* F induced by the rewards at the terminating

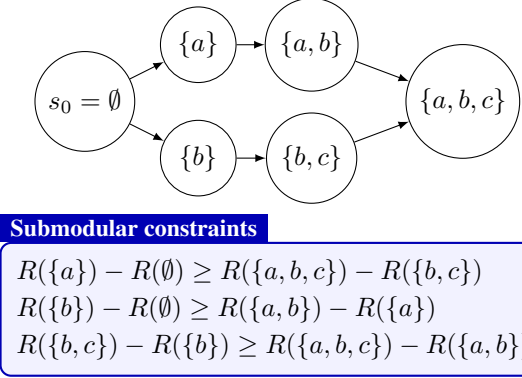


Figure 1. An example of a DAG with submodular reward. States are sets of elements, actions add an element to the current state. Submodularity constrains the reward of states, ensuring that there is a diminishing return over time for the reward of later states.

states through the DAG such that the incoming and outgoing flows match at every vertex of the DAG. That is, $F(x) = R(x)$, while the flows at intermediate states $F(s)$ and through edges $F(s \rightarrow s')$ is to be determined by the GFN by balancing *flow matching* equations in the DAG.

The forward and backward policies $P_F(s'|s)$ and $P_B(s|s')$ are key components of GFNs, as they model a distribution over transitions between states $s \rightarrow s'$. These policies may be parameterized directly or defined in terms of the flow function F over states and transitions (e.g. $P_F(s'|s) = F(s \rightarrow s')/F(s)$ and $P_B(s|s') = F(s' \rightarrow s)/F(s')$). A common approach to train a GFN is to start P_F at the initial state s_0 and let it generate a sequence of transitions (i.e. a trajectory) until it decides (or is forced) to stop in any terminating state $x \in \mathcal{X}$. Similarly, one may start P_B from a terminating state $x \in \mathcal{X}$ and let it generate sequences of transitions until it is forced to stop when s_0 is reached.

These trajectories are then used to compute a *loss* derived from various flow matching equations (Malkin et al., 2022; Deleu et al., 2022; Pan et al., 2023) in which the rewards are the *learning signals*. As in several prior works (Pan et al., 2023; Zhang et al., 2023a;b; Sendera et al., 2024), we assume rewards at intermediate states in a trajectory can be observed, in addition to rewards at terminating states.

4. Submodular Upper Bounds

In this section, we show that given a DAG with a submodular reward function (Assumption 3.1), one can obtain an upper bound on the reward for any terminating state. Given a finite dataset of trajectories, we then provide theoretical guarantees on the number of distinct upper bounds that can be obtained on a single terminating state, along with a lower bound on the number of distinct terminating state covered by an upper bound.

Property 4.1 (Submodular Upper Bounds). Given a submodular reward function (Assumption 3.1), we can obtain the following upper bound on the reward at terminating state $x \in \mathcal{X}$ given an intermediate state $s \subset x$ and an action a such that $a \in x$, but $a \notin s$:

$$R(x) \leq \text{UB}(x|s, a) := R(s \cup \{a\}) - R(s) + R(x \setminus \{a\}).$$

Because the marginal gain of adding element a diminishes as the set s grows, the value of adding a to a small intermediate set s is an overestimate (upper bound) of adding a to the final set x that becomes tighter as s becomes closer to x . Property 4.1 essentially states that intermediate rewards enable data-augmentation. In what follows, $\text{UB}(x)$ denotes an arbitrary upper bound on $R(x)$, and $\text{UB}(x)$ can be arbitrarily loose.

Computing upper bounds as in Property 4.1 requires a *dataset* of previously visited states $s \in \mathcal{S}$ along with their associated reward $R(s)$. To study the rate at which these upper bounds are generated, we assume the following:

Assumption 4.2 (Uniform Trajectory Collection). We assume the policy collecting trajectories to produce the dataset \mathcal{D} of pairs $(s, R(s))$ is a uniform distribution over the set of all possible trajectories \mathcal{T} , i.e., $P_F(\tau) = 1/|\mathcal{T}|, \forall \tau \in \mathcal{T}$.

As long as the probability of sampling each trajectory is non-zero, the results below still hold (at lower convergence rates). As a result, Assumption 4.2 can be relaxed to include the common ϵ -greedy sampling policy. Detailed derivations and proofs are deferred to Appendix A.

4.1. Generating Upper Bounds

Consider terminating state $x \in \mathcal{X}$, intermediate state $s \subset x$, and action a such that $a \in x$, but $a \notin s$. We denote $p_{x,a} := x \setminus \{a\}$ the *parent* of terminating state x from which element a is removed and note that since $|x| = C, \forall x \in \mathcal{X}$, there are C parents per terminating state. We observe that the states $p_{x,a}$ and $s \cup \{a\}$ cannot be encountered in the same trajectory. Therefore, computing an upper bound (Property 4.1) require sampling at least a *pair of trajectories* from \mathcal{T} . We establish the criteria for these trajectories in the following definitions.

Definition 4.3 (Parent trajectories). Given a terminating state x and its parent $p_{x,a}$, we denote $\mathcal{T}(p_{x,a})$ the set of trajectories passing through a parent of x and ending in a terminating state $x' \neq x$. Note that the number of parent trajectories $|\mathcal{T}(p_{x,a})|$ is identical for all x and a .

Definition 4.4 (Compatible trajectories). Given a terminating state x and its parent $p_{x,a}$ (Definition 4.3), we note $\tilde{\mathcal{T}}(p_{x,a})$ the set of trajectories passing through a state $s \subset p_{x,a}$, transition into $s \cup \{a\}$, and end in a terminating state $x' \neq x$. These trajectories are said to be *compatible*

with the trajectories in $\mathcal{T}(p_{x,a})$ as they jointly result into an upper bound on $R(x)$. Note that the number of compatible trajectories $|\tilde{\mathcal{T}}(p_{x,a})|$ is identical for all x and a .

Note that parent and compatible trajectories of terminating state x do not terminate in x , as this would mean observing $R(x)$, thus making the upper bound useless. Figure 2 illustrates an example of trajectories fitting each definition.

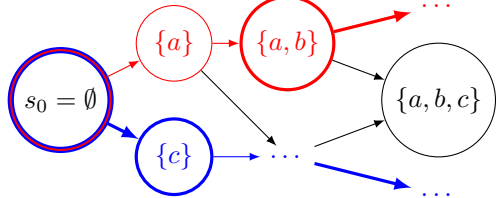


Figure 2. A subset of the DAG, showing an example pair of trajectories for $\mathcal{T}(p_{x,c})$ and $\tilde{\mathcal{T}}(p_{x,c})$ for $x = \{a, b, c\}$. This pair of trajectory yields the bound $\text{UB}(\{a, b, c\}|\emptyset, c) = R(\{c\}) - R(\emptyset) + R(\{a, b\})$. The \dots indicate an ellipsis in the DAG, where any number of valid transitions are taken. Bold edges and vertices highlight key elements in trajectory.

Trajectory-pairing graph Fixing a terminating state $x \in \mathcal{X}$, we exploit a graph representation $G(x) = (\mathcal{V}, \mathcal{E}(x))$ of the trajectories, where vertices $\mathcal{V} = \mathcal{T}$ correspond all possible trajectories and edges $\mathcal{E}(x) = \bigcup_{a \in x} \mathcal{T}(p_{x,a}) \times \tilde{\mathcal{T}}(p_{x,a})$ correspond to all pairs of parent-compatible trajectories that result in an upper bound on $R(x)$. Notice that $|\mathcal{E}(x)| = C|\mathcal{T}(p_{x,a})||\tilde{\mathcal{T}}(p_{x,a})|$, as each parent trajectory of x (Definition 4.3), for any of the C parents, can be paired with any of their respective compatible trajectories (Definition 4.4). We can now show how many distinct upper bounds on $R(x)$ can be obtained (in expectation) given a dataset of m uniformly sampled trajectories (Assumption 4.2).

Proposition 4.5 (Expected number of distinct upper bounds on the reward of a terminating state). *Let $Q(m)$ be the number of distinct bounds on any given terminal state x given a dataset of m trajectories (Assumption 4.2), then*

$$\begin{aligned} \mathbb{E}[Q(m)] \\ \in \Omega \left(N^C C! \left(1 - \frac{C-1}{N} \right)^{C-1} \left(1 - e^{-\frac{m}{N^C}} \right)^2 \right). \end{aligned}$$

Note that this is true for any terminating state x . Hence, every terminating state have the same expected number of distinct bounds, which grows with m , the number of uniformly collected trajectories. \square

Proof Sketch. This is obtained directly from the linearity of expectation applied on the number of edges in the subgraph induced by the m sampled trajectories. \square

Proposition 4.5 states that there may be more than a single upper bound available for a given terminating state x given a dataset of m trajectories. As a result, some upper bounds will be tighter (closer the true value $R(x)$) than others. In the following, unless specified, $\text{UB}(x)$ denotes the tightest bound available on $R(x)$.

4.2. Expected Coverage

We now turn our attention to how much of the terminating state space \mathcal{X} we can expect to *cover* with submodular upper bounds after m uniformly sampled trajectories (Assumption 4.2). To achieve this, we begin by recovering the probability of sampling trajectories such that a bound on $R(x)$ emerges, for any terminating state $x \in \mathcal{X}$. As two edges in the graph $G(x)$ may share a common vertex, we must account for the dependencies between the edges (and thus between different upper bounds for the same $R(x)$). Using classical results in probabilistic combinatorics, we obtain the following:

Theorem 4.6 (Probability of producing a submodular upper bound). *Let $Q(m)$ be the number of distinct upper bounds on the reward of a terminating state x for any $x \in \mathcal{X}$ given a dataset of m trajectories (Assumption 4.2). We have that*

$$\mathbb{P}(Q(m) > 0) \geq 1 - e^{-\Omega(\Lambda(m))}$$

where

$$\Lambda(m) := N(C-1)! \left(1 - \frac{C-1}{N} \right)^{2(C-1)} \left(1 - e^{-\frac{m}{N^C}} \right).$$

and N is the number of available actions while C is the cardinality constraint.

Proof Sketch. Leveraging the graph representation, we find the number of edges with a shared vertex in $G(x)$, then compute the total pairwise dependence between edges in $G(x)$ by summing the probability of co-occurrence of two edges with a shared vertex in m sampled trajectories. Combining this with Proposition 4.5, we obtain our result using Janson's Inequalities (Bollobás, 1988; Janson et al., 1988). \square

Theorem 4.6 indicates that the probability of having a submodular upper bound on $R(x)$ follows the complement of an exponential decay, but the specific rate at which it grows depends on N and C . This leads us to the following result for the lower bound on the expected coverage of \mathcal{X} .

Corollary 4.7 (Expected coverage of terminating state space). *Let $\kappa(m)$ denote the number of terminating states covered by a submodular upper bound given a dataset of m trajectories (Assumption 4.2). Then given $\Lambda(m)$ (Theorem 4.6) we have that*

$$\mathbb{E}[\kappa(m)] \geq \binom{N}{C} \left(1 - e^{-\Omega(\Lambda(m))} \right).$$

Proof Sketch. This result follows from a direct application of the definition of expectation. \square

5. SUBO-GFN

We introduce **Submodular Upper-Bounds GFN** (SUBO-GFN), an approach that leverages the submodular upper bounds (Property 4.1) to transform a single query to the reward function into multiple upper bounds (given a dataset of trajectories). Following the OFU principle (Brafman & Tennenholtz, 2002), SUBO-GFN learns both from the rewards of the observed states and on the upper bounds of unobserved terminating states. We show that this improves the amount of information that can be extracted from individual trajectories, improving data efficiency. We then show that the optimism of the upper bounds leads the learned distribution to induce oversampling on highly uncertain, unobserved terminating states, thus improving exploration.

5.1. Data Efficiency

A fair question is whether SUBO-GFN covers more of the terminating state space \mathcal{X} per query to the reward function than classical GFNs. First, we note that GFN policies are highly entropic, roughly approaching a uniform distribution at initialization and during early training (Shen et al., 2023a). Additionally, it is often the case that trajectories are collected by a mixture of the learned policy P_F and a uniform distribution (e.g. ϵ -greedy) (Shen et al., 2023a). As such, Assumption 4.2 (and thus Corollary 4.7) are expected to hold on such GFN-sampled trajectories.

Recall that learning signals in classical GFNs (Bengio et al., 2023) are typically limited to rewards queried at terminating states, whereas SUBO-GFN can also query rewards at intermediate states. Assuming SUBO-GFN observes a total of mC rewards in m trajectories, as a result of observing intermediate rewards, then a classical GFN could observe up to mC terminating states and their rewards in the same number of queries to the reward function. As Corollary 4.7 highlights, a key quantity for the coverage $\kappa(m)$ is the ratio between the cardinality constraint C and the number of available actions N .

Figure 3 displays the relationship between C/N and the ratio $\kappa(m)/mC$ for different number of trajectories m . All points above the black dashed line are situations where using SUBO-GFN is worthwhile, as the mC queries to R allow it to cover more than mC terminating states using upper bounds. **In most scenarios of interest, where $C \ll N$, submodular upper bounds are data-efficient, covering a large portion of \mathcal{X} with relatively few queries to R .** This is in stark contrast to classical GFN training where there is a 1-to-1 ratio (one query to R gives learning signal on a single $x \in \mathcal{X}$). In other words, in proportion, SUBO-GFN turns a

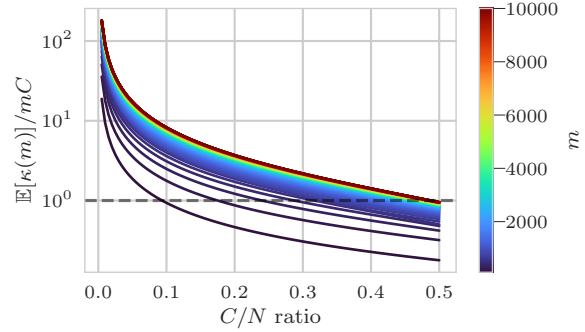


Figure 3. Normalized coverage (using Theorem A.16) as a function of the cardinality-actions ratio and the number of uniformly sampled trajectories (Assumption 4.2). As C/N decreases, submodular upper bounds covers order of magnitudes more terminating states than would a classical GFN. The black dashed line represents the 1 : 1 ratio between query and coverage. Points above this line represent scenarios where SUBO-GFN is worthwhile.

single query to the reward function at an intermediate state into multiple learning signals over the terminating states \mathcal{X} via the upper bounds.

5.2. Sampling Distribution Bias

Let P denote the target sampling distribution, with $P(x) := R(x)/Z$ being the target probability of sampling terminating state $x \in \mathcal{X}$, and let \tilde{P} denote the learned sampling distribution. We analyze the bias induced in the learned sampling distribution when jointly learning from upper bounds and observed rewards, at the point where all unobserved terminating states have been assigned an upper bound. Let $\mathcal{X}_{UB} \subset \mathcal{X}$ and $\bar{\mathcal{X}}_{UB} = \mathcal{X} \setminus \mathcal{X}_{UB}$ respectively denote the set of unobserved terminating states, which are characterized by their upper bound, and the set of observed terminating states, for which the true reward is known. Defining the *optimism gap* $\Delta(x) := UB(x) - R(x)$ at terminating state $x \in \mathcal{X}_{UB}$, we observe that jointly learning from rewards on $\bar{\mathcal{X}}_{UB}$ and upper bounds on \mathcal{X}_{UB} induces the optimistic partition function

$$\tilde{Z} := \sum_{x \in \mathcal{X}_{UB}} UB(x) + \sum_{x \in \bar{\mathcal{X}}_{UB}} R(x) = Z + \sum_{x \in \mathcal{X}_{UB}} \Delta(x) \quad (1)$$

and the resulting biased sampling distribution

$$\tilde{P}(x) := \begin{cases} UB(x)/\tilde{Z} & \text{for } x \in \mathcal{X}_{UB} \\ R(x)/\tilde{Z} & \text{for } x \in \bar{\mathcal{X}}_{UB}. \end{cases} \quad (2)$$

Given any terminating state $x \in \mathcal{X}$, we say that oversampling occurs when the probability of sampling x under the learned distribution dominates the probability of sampling x under the target distribution, that is $\tilde{P}(x) \geq P(x)$.

Theorem 5.1 (Optimism-Induced Oversampling). *Learning from upper bounds results in oversampling of the unob-*

served terminating state $x \in \mathcal{X}_{UB}$ if and only if

$$\frac{(1 - P(x))}{P(x)} \Delta(x) \geq \sum_{x' \in \mathcal{X}_{UB} \setminus \{x\}} \Delta(x').$$

Proof Sketch. This result is obtained by using the definitions of $P(x)$, $\tilde{P}(x)$, and \tilde{Z} in $\tilde{P}(x) \geq P(x)$, and rearranging terms using simple algebraic manipulations (see Appendix A.4 for details). \square

Theorem 5.1 shows that in order for unobserved terminating states to have an increased sampling probability under the learned distribution \tilde{P} they need 1) their sampling probability under the target distribution P to be low; and 2) their upper bound to be sufficiently optimistic, i.e., have large optimism gaps. Intuitively, for two terminating states $x, x' \in \mathcal{X}_{UB}$ with $\Delta(x) = \Delta(x')$, the terminating state with the lowest sampling probability according to the true distribution will be favoured. Alternatively, for two terminating states $x, x' \in \mathcal{X}_{UB}$ with $P(x) = P(x')$, the terminating state with the largest optimism gap will be favoured, resulting in the exploration of high uncertainty terminating states. Naturally, oversampling some terminating states comes at the price of undersampling some other terminating states. By definition of $\tilde{P}(x)$ (Equation 2), all observed terminating states are undersampled, that is $\tilde{P}(x) < P(x) \forall x \in \tilde{\mathcal{X}}_{UB}$. However, the next experiments show that the resulting bias is negligible compared to the amount of information obtained from the upper bounds, as SUBO-GFN collapses more effectively to the target sampling distribution.

6. Experiments

We now conduct experiments to evaluate the potential of SUBO-GFN against a classical GFN (Bengio et al., 2021; Malkin et al., 2022) as baseline. We consider tasks inspired by the classical maximum set cover problem, which has a submodular structure. Specifically, we consider graph-based tasks, where given a graph, the action space \mathcal{A} corresponds to adding one vertex from the graph to the current set (state), while the state space \mathcal{S} corresponds to all the possible sets of vertices under the cardinality constraint C . Let $\mathcal{N}(a)$ denote the neighbouring vertices that can be reached from vertex $a \in \mathcal{A}$. The reward $R(s) = |\bigcup_{a \in s} \mathcal{N}(a)|/N$ of a given state $s \in \mathcal{S}$ corresponds to the (normalized) number of unique neighbours that can be reached by following the edges of the vertices in s , where $N = |\mathcal{A}|$.

Benchmark First, we investigate synthetic instances using random Erdős–Rényi (ER) and Barabási–Albert (BA) graphs, with a number of vertices $N = 1000$, as they are commonly used in synthetic submodular tasks such as influence maximization (Zhang et al., 2025) (see Appendix B for details). We also conduct experiments on real-world

graph datasets: Cora (Yang et al., 2016), CiteSeer (Yang et al., 2016), and GrQc (Leskovec et al., 2007). GrQc is the largest instance, with $N = 5249$ vertices, whereas CiteSeer and Cora have $N = 3279$ and $N = 2708$ respectively. The reward landscape is defined by the graph connectivity. As such, even if the reward is defined in the same way, each instance has a vastly different reward distribution. We consider cardinality constraints $C \in \{5, 10, 15\}$ for all tasks. This ensures that the problem instances are large without inducing issues with credit assignment due to long trajectories. As the difficulty of an instance increases with the cardinality constraint C (as this increases the set of terminating states \mathcal{X}), we limit ourselves to results for $C = 15$ in the main paper and defer results on easier instance ($C \in \{5, 10\}$) to Appendix C.

Metrics For each experiment, we measure the Flow Consistency in Subgraph (FCS) (Silva et al., 2024). Introduced as a tractable proxy for the Total Variation (TV) distance between the learned distribution \tilde{P} and the target distribution P . We also report the Top-100 Average Reward, which is a classical application-focused performance measure for GFNs. We report additional results on the loss and the number of bounds generated by SUBO-GFN to Appendix C.

Methodology For each experiment, a total of 10,000 queries to R are allowed. Restricting the query budget allows fair comparison between the classical GFN, which queries R once per trajectory, and SUBO-GFN, which observes intermediate state rewards. Once the query budget is exhausted, we continue training all GFNs *offline* on their accumulated data. This allows to further monitor the learning signals that can be obtained using upper bounds. We present the results with respect to the gradient steps to observe the progress of training beyond the fixed number of trajectories that can be sampled. Each experiment is repeated 10 times on a different random seed; we report the mean and 95% confidence intervals (computed from a t distribution). In experiments on random graphs, note that graph instances are also randomized by the seed, such that results are aggregated on 10 graph instances.

Implementation Details We implement SUBO-GFN such that it only considers the tightest bound available in each given state and filters out upper bounds below the highest reward observed so far. This limits exploration to promising states only. After budget exhaustion, this filtering is turned off to prevent overfitting. We investigate the SUBO-GFN-F variant, for which the filtering remains. This forces SUBO-GFN-F to exploit its knowledge and focus the flow where the reward seems to improve over the highest reward so far. As in prior works (Zhang et al., 2023b; Silva et al., 2024; Da Silva et al., 2024), we parameterize all strategies with a Graph Isomorphism Network (Xu et al.,

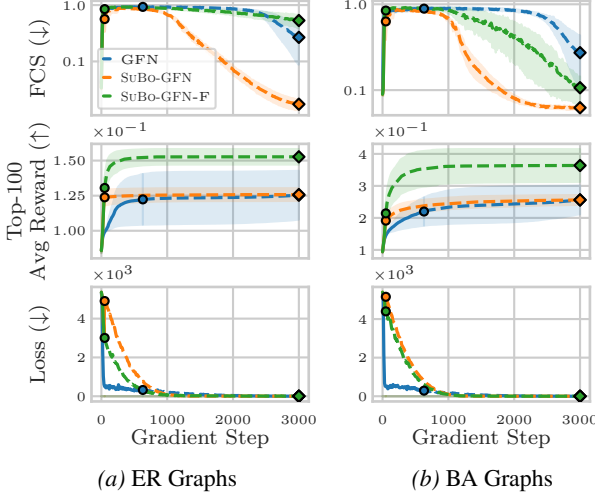


Figure 4. Performance metrics and training loss of the classical GFN and SUBO-GFN variants on random graphs. Strategies are trained online (plain line) until the \bullet marker, then trained offline (dashed line) without further queries to R until the end of the experiment indicated by the \blacklozenge marker.

2018). All GFNs are trained off-policy using the Trajectory Balance criterion (Malkin et al., 2022), with a replay buffer accumulating sampled trajectories; SUBO-GFN variants additionally consider submodular upper bounds on the reward of unobserved terminating states. See Appendix D for more details.

6.1. Random Graphs

Figure 4 displays the FCS and the Top-100 Average Reward over gradient steps, along with the learning loss reported as a reference, on 10 random instances of ER and BA graphs with cardinality constraint $C = 15$.

We observe that SUBO-GFN improves distribution matching (decreases FCS) much faster than the classical GFN baseline. Looking at the loss, we observe that reducing the loss is much more indicative of reducing the FCS for SUBO-GFN than it is for the classical GFN. This is likely directly due to the sheer amount of data SUBO-GFN trains on, preventing overfitting. Indeed, classical GFN is limited to 10,000 training data, which SUBO-GFN greatly inflates by leveraging the problem structure to compute upper bounds. Indeed, Figure 11 (Appendix C) shows there are more than 3×10^5 terminating states with an upper bound at the beginning of the offline training phase for SUBO-GFN(-F). We observe that SUBO-GFN-F, which only focuses on a small fraction of the upper bounds during offline training, is not able to improve distribution matching as much.

SUBO-GFN is also competitive with classical GFNs in terms of Top-100 Average Reward, while having much tighter confidence intervals across experiment. This indi-

cates that SUBO-GFN is much more consistent. Strictly learning to allocate flow where there is promise to increase the best observed reward seems to advantage SUBO-GFN-F, as it performs best in terms of Top-100 Average Reward, at the cost of FCS.

Easier instances Figures 9 and 10 (Appendix C) show a trend where, as the cardinality constraint C grows, the classical GFN struggles with distribution matching, but catches up to SUBO-GFN(-F) in Top-100 Average Reward. SUBO-GFN exhibit strong performance in distribution matching regardless of the cardinality constraint C .

6.2. Real-World Graphs

Figure 5 displays the FCS and the Top-100 Average Reward over gradient steps on real-world graphs extracted from datasets Cora (Yang et al., 2016), CiteSeer (Yang et al., 2016), and GrQc (Leskovec et al., 2007), with cardinality constraint $C = 15$.

Similarly to previous results, distribution matching improves (FCS decreases) much faster when using SUBO-GFN. The volume of training data is likely to be the driving factor here once again, as Figure 14 (Appendix C) shows there are nearly 4×10^5 terminating states with an upper bound at the beginning of the offline training phase. In terms of Top-100 Average Reward, we note once again that SUBO-GFN remains comparable to the classical GFN, while SUBO-GFN-F sometimes significantly outperforms classical GFN as it specializes in attributing flow in promising areas of the state space.

Easier instances Figures 12 and 13 (Appendix C) show that, as the instances become larger, SUBO-GFN-F seems to outpace classical GFNs. As such, SUBO-GFN offers once again a better trade-off between distribution matching and high-reward candidate generation.

6.3. Discussion

SUBO-GFN achieves superior distribution matching (lower FCS) without compromising on the quality of sampled candidates (Top-100 Average Reward) and with lower variance. Furthermore, continuing filtering during offline training (with SUBO-GFN-F) specializes SUBO-GFN for high-reward candidate generation, either competing with or outperforming classical GFNs. These gains persist across scales ($N \in \{1000, 2708, 3269, 5249\}$, $C \in \{5, 10, 15\}$), suggesting that structured rewards can unlock the potential of GFN in combinatorial domains. Although the instances are too large to fathom that SUBO-GFN learns the entire distribution, these results suggest that (constrained) data-augmentation with uncertain data (SUBO-GFN being a specific case) seems to help GFNs reduce the distance to

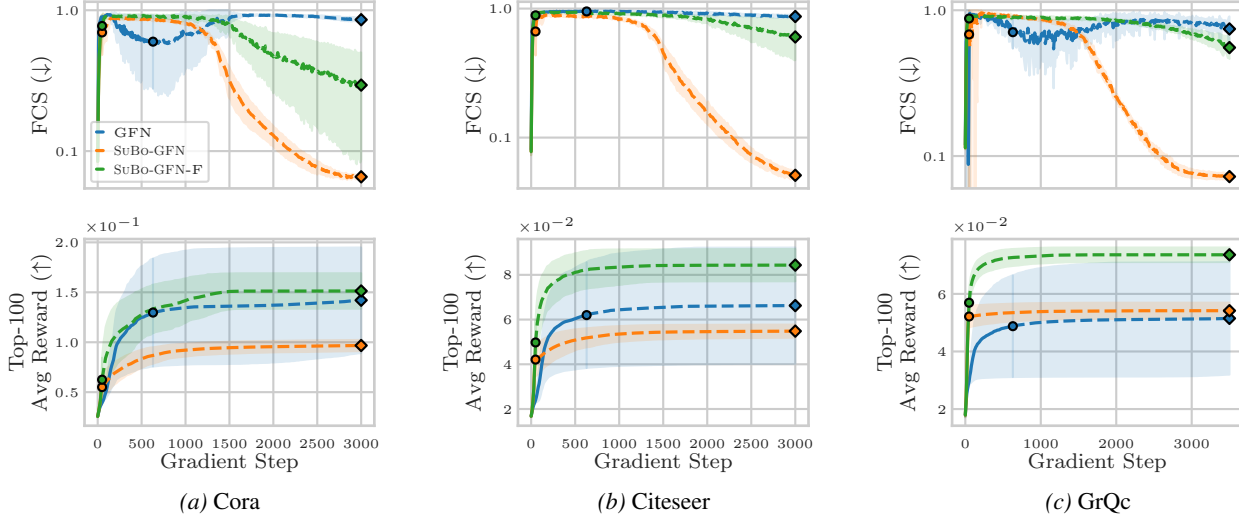


Figure 5. Performance metrics of the classical GFN and SUBO-GFN variants on real-world graphs. Strategies are trained online (plain line) until the \bullet , then trained offline (dashed line) without further queries to R until the end of the experiment indicated by the \blacklozenge .

the target distribution faster without sacrificing their performance from an applicative standpoint. Of particular interest is the fact that although the upper bounds on the reward stem from the structure of the reward, they can be arbitrarily loose. Despite this, SUBO-GFN allocates its flow much more efficiently than its classical counterpart. This raises questions, notably on how much uncertainty can be tolerated by GFNs such that they still learn approximately the right distribution in practice. These results also suggest that data scale is the most important factor in learning the target, a long-held intuition in the field (Halevy et al., 2009).

7. Conclusion

In this work, we study how the structure of the reward function in GFNs can be exploited. We first theoretically investigate how submodularity can be harnessed to retrieve upper bounds on the reward of unobserved terminating states. We show that the expected number of distinct upper bounds that can be generated for a given terminating state grows exponentially with the number of trajectories in the dataset (Proposition 4.5). Accordingly, we show that the probability of generating at least one upper bound of a given terminating state also grows exponentially with the number of sampled trajectories (Theorem 4.6), and further provide a result on the expected coverage of the terminating state space by upper bounds (Corollary 4.7).

Following the OFU principle, we then introduce SUBO-GFN, an approach which leverages the submodular upper bounds on unobserved terminating states to train a GFN. SUBO-GFN produces *orders of magnitude* more training data than classical GFNs for the same number of queries to the reward function. We further show that the optimistic na-

ture of SUBO-GFN biases the learned distribution towards oversampling unobserved terminating states with high uncertainty or low sampling probability (Theorem 5.1).

We empirically demonstrate that SUBO-GFN improves distribution matching faster than classical GFNs without sacrificing high-quality candidate generation for applicative purposes. While we focus on graph-based tasks here, SUBO-GFN is applicable to *any* problem with a submodular reward (e.g. facility location, sensor selection, feature selection). Our empirical results raise questions notably on how much uncertainty GFNs can tolerate while still achieving the desired behaviour in practice.

Limitations and Future Work While we provide in-depth analyses when trajectories are collected uniformly, integrating the GFN interactive learning loop in the generation of upper bounds presents a promising extension. Theoretical results could be further strengthened by considering trajectory splicing, where two sub-trajectories are merged, to produce more compatible trajectories for a parent trajectory. Additionally, the various possible rearrangements of Assumption 3.1 suggest that extending submodular bounds to the full state space could enable scaling beyond current limits. Beyond submodularity, extending our understanding of useful mechanisms for GFNs on well-understood reward structures is an interesting prospect.

8. Acknowledgements

We acknowledge the support of CIFAR, the DEEL Project, of the Natural Sciences and Engineering Research Council of Canada (NSERC), [BESC D-589331 - 2024] and of the Fonds de Recherche du Québec Nature et Technologies

[344232]. Furthermore, this research was enabled in part by support provided by Calcul Québec (calculquebec.ca) and the Digital Research Alliance of Canada (alliancecan.ca). The authors would also like to acknowledge the valuable insights provided by Amer Essakine and Julien Armand in the development of the proofs.

9. Impact Statement

This paper presents work whose goal is to advance the field of machine learning. There are many potential societal consequences of our work, none of which we feel must be specifically highlighted here.

References

Auer, P. and Ortner, R. Logarithmic Online Regret Bounds for Undiscounted Reinforcement Learning. In *Advances in Neural Information Processing Systems*, volume 19. MIT Press, 2006.

Auer, P., Cesa-Bianchi, N., and Fischer, P. Finite-time Analysis of the Multiarmed Bandit Problem. *Machine Learning*, 47(2):235–256, 2002.

Azar, M. G., Osband, I., and Munos, R. Minimax Regret Bounds for Reinforcement Learning. In *Proceedings of the 34th International Conference on Machine Learning*, pp. 263–272. PMLR, 2017.

Bengio, E., Jain, M., Korablyov, M., Precup, D., and Bengio, Y. Flow Network based Generative Models for Non-Iterative Diverse Candidate Generation. In *Advances in Neural Information Processing Systems*, volume 34, pp. 27381–27394. Curran Associates, Inc., 2021.

Bengio, Y., Lahlou, S., Deleu, T., Hu, E. J., Tiwari, M., and Bengio, E. GFlowNet Foundations. *Journal of Machine Learning Research*, 24(210):1–55, 2023.

Bollobás, B. The chromatic number of random graphs. *Combinatorica*, 8(1):49–55, 1988.

Brafman, R. I. and Tennenholz, M. R-MAX - A General Polynomial Time Algorithm for Near-Optimal Reinforcement Learning. *Journal of Machine Learning Research*, 3(Oct):213–231, 2002.

Chen, Y. and Mauch, L. Order-Preserving GFlowNets. In *The Twelfth International Conference on Learning Representations*, October 2023.

Da Silva, T., Carvalho, L. M., Souza, A., Kaski-Diego Mesquita, S., and Mesquita, D. Embarrassingly parallel GFlowNets. In *Proceedings of the 41st International Conference on Machine Learning*, volume 235, pp. 45406–45431. JMLR, 2024.

Dann, C., Lattimore, T., and Brunskill, E. Unifying PAC and Regret: Uniform PAC Bounds for Episodic Reinforcement Learning. In *Advances in Neural Information Processing Systems*, volume 30. Curran Associates, Inc., 2017.

Deleu, T., Góis, A., Emezue, C., Rankawat, M., Lacoste-Julien, S., Bauer, S., and Bengio, Y. Bayesian structure learning with generative flow networks. In *Proceedings of the Thirty-Eighth Conference on Uncertainty in Artificial Intelligence*, pp. 518–528. PMLR, 2022.

Domingos, P. and Richardson, M. Mining the network value of customers. In *Proceedings of the Seventh ACM SIGKDD International Conference on Knowledge Discovery and Data Mining*, KDD ’01, pp. 57–66, New York, NY, USA, 2001. Association for Computing Machinery.

Evmorfo, S., Xu, Z., and Petropulu, A. Gflownets for Sensor Selection. In *2023 IEEE 33rd International Workshop on Machine Learning for Signal Processing (MLSP)*, pp. 1–6, Rome, Italy, 2023. IEEE.

Gasperini, M., Hill, A. J., McFadie-Figueroa, J. L., Martin, B., Kim, S., Zhang, M. D., Jackson, D., Leith, A., Schreiber, J., Noble, W. S., et al. A genome-wide framework for mapping gene regulation via cellular genetic screens. *Cell*, 176(1):377–390, 2019.

Halevy, A., Norvig, P., and Pereira, F. The Unreasonable Effectiveness of Data. *IEEE Intelligent Systems*, 24(2): 8–12, 2009.

Jain, M., Bengio, E., Hernandez-Garcia, A., Rector-Brooks, J., Dossou, B. F. P., Ekbole, C. A., Fu, J., Zhang, T., Kilgour, M., Zhang, D., Simine, L., Das, P., and Bengio, Y. Biological Sequence Design with GFlowNets. In *Proceedings of the 39th International Conference on Machine Learning*, pp. 9786–9801. PMLR, 2022.

Jang, H., Kim, M., and Ahn, S. Learning Energy Decompositions for Partial Inference in GFlowNets. In *The Twelfth International Conference on Learning Representations*, 2023.

Janson, S., Luczak, T., and Rucinski, A. An Exponential Bound for the Probability of a Specified Subgraph in a Random Graph. 1988.

Kim, M., Yun, T., Bengio, E., Zhang, D., Bengio, Y., Ahn, S., and Park, J. Local Search GFlowNets. In *The Twelfth International Conference on Learning Representations*, 2023.

Koziarski, M., Rekesh, A., Shevchuk, D., van der Sloot, A. M., Gaiński, P., Bengio, Y., Liu, C.-H., Tyers, M., and Batey, R. A. RGFN: Synthesizable Molecular Generation Using GFlowNets. In *The Thirty-eighth Annual*

Conference on Neural Information Processing Systems, 2024.

Leskovec, J., Kleinberg, J., and Faloutsos, C. Graph evolution: Densification and shrinking diameters. *ACM Trans. Knowl. Discov. Data*, 1(1):2–es, 2007.

Li, L., Chu, W., Langford, J., and Schapire, R. E. A contextual-bandit approach to personalized news article recommendation. In *Proceedings of the 19th International Conference on World Wide Web*, WWW ’10, pp. 661–670, New York, NY, USA, 2010. Association for Computing Machinery.

Ma, G., Bengio, E., Bengio, Y., and Zhang, D. Baking Symmetry into GFlowNets. In *NeurIPS 2023 AI for Science Workshop*, 2023.

Madan, K., Lamb, A., Bengio, E., Berseth, G., and Bengio, Y. Towards Improving Exploration through Sibling Augmented GFlowNets. In *The Thirteenth International Conference on Learning Representations*, 2024.

Malkin, N., Jain, M., Bengio, E., Sun, C., and Bengio, Y. Trajectory balance: Improved credit assignment in GFlowNets. In *Advances in Neural Information Processing Systems*, 2022.

Metropolis, N., Rosenbluth, A. W., Rosenbluth, M. N., Teller, A. H., and Teller, E. Equation of state calculations by fast computing machines. *The journal of chemical physics*, 21(6):1087–1092, 1953.

Mistal, Hernández-García, A., Volokhova, A., Duval, A. A., Bengio, Y., Sharma, D., Carrier, P. L., Koziarski, M., and Schmidt, V. Crystal-GFN: Sampling materials with desirable properties and constraints. In *AI for Accelerated Materials Design - NeurIPS 2023 Workshop*, 2023.

Pan, L., Zhang, D., Courville, A., Huang, L., and Bengio, Y. Generative Augmented Flow Networks. In *The Eleventh International Conference on Learning Representations*, 2022.

Pan, L., Malkin, N., Zhang, D., and Bengio, Y. Better Training of GFlowNets with Local Credit and Incomplete Trajectories. In *Proceedings of the 40th International Conference on Machine Learning*, pp. 26878–26890. PMLR, 2023.

Rector-Brooks, J., Madan, K., Jain, M., Korablyov, M., Liu, C.-H., Chandar, S., Malkin, N., and Bengio, Y. Thompson Sampling for Improved Exploration in GFlowNets. In *ICML 2023 Workshop on Structured Probabilistic Inference \& Generative Modeling*, 2023.

Sendera, M., Kim, M., Mittal, S., Lemos, P., Scimeca, L., Rector-Brooks, J., Adam, A., Bengio, Y., and Malkin, N. Improved off-policy training of diffusion samplers. In Globerson, A., Mackey, L., Belgrave, D., Fan, A., Paquet, U., Tomczak, J., and Zhang, C. (eds.), *Advances in Neural Information Processing Systems*, volume 37, pp. 81016–81045. Curran Associates, Inc., 2024.

Seo, S., Kim, M., Shen, T., Ester, M., Park, J., Ahn, S., and Kim, W. Y. Generative Flows on Synthetic Pathway for Drug Design. *CoRR*, 2024.

Shamaiah, M., Banerjee, S., and Vikalo, H. Greedy sensor selection: Leveraging submodularity. In *49th IEEE Conference on Decision and Control (CDC)*, pp. 2572–2577, 2010.

Shen, M. W., Bengio, E., Hajiramezanali, E., Loukas, A., Cho, K., and Biancalani, T. Towards Understanding and Improving GFlowNet Training. In *Proceedings of the 40th International Conference on Machine Learning*, pp. 30956–30975. PMLR, 2023a.

Shen, T., Pandey, M., and Ester, M. TacoGFN: Target Conditioned GFlowNet for Drug Design. In *NeurIPS 2023 Generative AI and Biology (GenBio) Workshop*, 2023b.

Silva, T., Alves, R. B., da Silva, E. d. S., Souza, A. H., Garg, V., Kaski, S., and Mesquita, D. When do GFlowNets learn the right distribution? In *The Thirteenth International Conference on Learning Representations*, 2024.

Xu, K., Hu, W., Leskovec, J., and Jegelka, S. How Powerful are Graph Neural Networks? In *International Conference on Learning Representations*, 2018.

Yang, Z., Cohen, W., and Salakhudinov, R. Revisiting Semi-Supervised Learning with Graph Embeddings. In *Proceedings of The 33rd International Conference on Machine Learning*, pp. 40–48. PMLR, 2016.

Zhang, D., Chen, R. T. Q., Liu, C.-H., Courville, A., and Bengio, Y. Diffusion Generative Flow Samplers: Improving learning signals through partial trajectory optimization. In *The Twelfth International Conference on Learning Representations*, 2023a.

Zhang, D., Dai, H., Malkin, N., Courville, A., Bengio, Y., and Pan, L. Let the Flows Tell: Solving Graph Combinatorial Problems with GFlowNets. In *Thirty-Seventh Conference on Neural Information Processing Systems*, 2023b.

Zhang, D. W., Rainone, C., Peschl, M., and Bondesan, R. Robust Scheduling with GFlowNets. In *The Eleventh International Conference on Learning Representations*, 2022.

Zhang, Z., Li, D., Wang, Y., Chen, W., and Zhu, Y. Sequential decision based learning method for influence maximization. *Theoretical Computer Science*, 1036:115147, 2025.

Zhou, D., Li, L., and Gu, Q. Neural Contextual Bandits with UCB-based Exploration. In *Proceedings of the 37th International Conference on Machine Learning*, pp. 11492–11502. PMLR, 2020.

A. Proofs

As most of our proofs rely on the size of parent $p_{x, \cdot}$, we define $K = C - 1$. In addition to Assumption 4.2, we also rely on the following assumption.

Assumption A.1. Given the cardinality constraint C and $N = |\mathcal{A}|$, we assume $C \leq N/2$. This implies $K \leq N/2 - 1 \leq N/2$.

This assumption is mild, as binomial coefficients $\binom{N}{C}$ are symmetric, and peak at $C = \lfloor N/2 \rfloor$, according to Sperner's theorem.

Furthermore, we rely on a graph representation of the trajectories and their relationships. Specifically, we fix a terminating state $x \in \mathcal{X}$ and define $G(x) = (\mathcal{V}, \mathcal{E}(x))$ of the trajectories, where vertices correspond to the set of all possible trajectories, $\mathcal{V} = \mathcal{T}$, and edges $\mathcal{E}(x) = \bigcup_{a \in x} \mathcal{T}(p_{x,a}) \times \tilde{\mathcal{T}}(p_{x,a})$. That is to say, $\mathcal{E}(x)$ consists of pairs of trajectories (τ_i, τ_j) , $\tau_i, \tau_j \in \mathcal{T}$ that result in an upper bound on $R(x)$. The graph has the same shape for any chosen x , but the edges vary based on x . In the following, we provide proofs for a fixed arbitrary $x \in \mathcal{X}$. Since the graph's structural properties are the same regardless of x , we apply our result to all of \mathcal{X} .

A.1. Proof of Theorem 4.5

First, recall the set of all trajectories \mathcal{T} . There are $\frac{N!}{(N-C)!} = \frac{N!}{(N-K-1)!}$ trajectories in \mathcal{T} , obtained directly from the permutations formula. We find the following asymptotic lower bound for $|\mathcal{T}|$.

Lemma A.2. *Let \mathcal{T} be the set of trajectories in the DAG, then $|\mathcal{T}| \in O(N^{K+1})$*

Proof.

$$|\mathcal{T}| = \frac{N!}{(N-K-1)!} \leq N^{K+1} \implies |\mathcal{T}| \in O(N^{K+1}) \quad (3)$$

□

A.1.1. HOW MANY TRAJECTORIES FIT DEFINITION 4.3?

Let us first investigate how many trajectories pass through a single parent $p_{x,a}$. The following proposition states the result.

Proposition A.3 (Number of trajectories passing through a parent). *Let $p_{x,a}$ be an arbitrary parent of x and λ be the number of trajectories passing through $p_{x,a}$, then*

$$\lambda := K!(N - K - 1).$$

This quantity is identical for all x and a .

Proof. There are $K!$ permutations that reach $p_{x,a}$, since the parent contains K elements, and then any transition that does not lead to x can be chosen out of the $N - K$ remaining possible transitions. Since a single transition out of the parent leads to x , we get $(N - K - 1)$ possible transitions, yielding our result. □

We then compute the number of trajectories passing through any parent of terminating state $x \in \mathcal{X}$.

Proposition A.4 (Number of trajectories passing through any parent of a terminating state). *Let α be the number of trajectories passing through a parent, then*

$$\alpha := (K + 1)K!(N - K - 1) = (K + 1)!(N - K - 1)$$

This quantity is identical for all x and a .

Proof. Since there are $C = K + 1$ parent for any given x , we can simply multiply λ by $K + 1$, yielding our result. □

A.1.2. HOW MANY TRAJECTORIES FIT DEFINITION 4.4

Proposition A.5. Let $p_{x,a}$ be a parent of the terminating state $x \in \mathcal{X}$, and let β be the number of trajectories respecting Definition 4.4 for this parent, then

$$\beta = \prod_{i=0}^{K-1} (N-i) - (K+1)!$$

Proof. Let us fix $p_{x,a}$, a parent of x . By definition $a \notin p_{x,a}$. We now investigate how many trajectories are compatible with a trajectory passing through $p_{x,a}$. We proceed in an algorithmic fashion as follows.

1. Fixing $s \subset p_{x,a}$, $|s| = L < K$, how many trajectories pass through s and then pick element a ?
 - There are $L!$ sub-trajectories leading to s ;
 - Then, a single transition is taken (selecting element a);
 - Then, we can select $K+1-(L+1)=K-L$ elements out of $N-(L+1)$ elements;
 - This results in $\frac{(N-L-1)!}{(N-K-1)!}$ sub-trajectories out of $s \cup \{a\}$, since $N-K-1$ elements can be permuted out of $N-L-1$ elements;
 - Combining, we get $L! \frac{(N-L-1)!}{(N-K-1)!}$ trajectories passing through s and selecting element a .
2. For a fixed $L < K$, how many $s \subset p_{x,a}$ exist such that $|s| = L$?
 - Since we can combine any L elements out of K elements in the parent $p_{x,a}$, there are $\binom{K}{L}$ such sets.
3. Finally, notice that for every $s \subset p_{x,a}$, some of the trajectories passing through $s \cup \{a\}$ may also pass through $x = p_{x,a} \cup \{a\}$.
 - After transition $s \rightarrow s \cup \{a\}$, we can permute any element in $x \setminus s \cup \{a\}$. Thus, $K+1-L-1 = K-L$ elements that can be permuted;
 - Thus, there is a total of $L!(K-L)!$ trajectories that reach s , then choose $\{a\}$, then eventually end in x .
 - These trajectories must be subtracted, as they give $R(x)$, and thus render the computation of a bound useless.

We then sum these quantities for every $L \leq K-1$. As such, the number of trajectories that pass through ANY $s \subset p_{x,a}$ and selecting *specifically* a such that a bound on $x = p_{x,a} \cup \{a\}$ is discovered is:

$$\begin{aligned} \beta &:= \sum_{L=0}^{K-1} \binom{K}{L} L! \left[\frac{(N-L-1)!}{(N-K-1)!} - (K-L)! \right] = \sum_{L=0}^{K-1} \frac{K!}{(K-L)!} \left[\frac{(N-L-1)!}{(N-K-1)!} - (K-L)! \right] \\ &= \sum_{L=0}^{K-1} K! \left[\frac{(N-L-1)!}{(K-L)!(N-K-1)!} - 1 \right] \\ &= K! \sum_{L=0}^{K-1} \left[\binom{N-L-1}{K-L} - 1 \right] \end{aligned}$$

With the Hockey Stick Identity (HSI), we can reshape β to be more concise. The HSI states

$$\sum_{i=0}^{k-1} \binom{c+i}{i} = \binom{k+c}{k-1}, \quad n, r \in \mathbb{N}, n \geq r.$$

Let $i := K-L$, which implies $L = K-i$, we can deduce that $c+i = N-L-1 = N-K-1+i$ and thus $c = N-K-1$. We can then rewrite the sum in β so that it is now with respect to i . Notice that $L=0 \implies i=K$ and $L=K-1 \implies i=1$. The rewritten form is:

$$\sum_{i=1}^K \binom{N-K-1+i}{i} = \sum_{i=0}^K \binom{N-K-1+i}{i} - 1.$$

We leverage the identity to obtain

$$\begin{aligned} \sum_{L=0}^{K-1} \binom{N-L-1}{K-L} &= \sum_{i=0}^K \binom{N-K-1+1}{i} - 1 \\ &= \binom{N}{K} - 1. \end{aligned}$$

and deduce that $\sum_{L=0}^{K-1} 1 = K$.

Replacing in the definition of β , we get

$$\begin{aligned} \beta &= K! \left[\binom{N}{K} - K - 1 \right] \\ &= N(N-1)(N-2) \dots (N-K+1) - K!(K+1) \\ &= \prod_{i=0}^{K-1} (N-i) - (K+1)! \end{aligned}$$

□

A.1.3. NUMBER OF DISTINCT BOUNDS FOR THE REWARD OF A TERMINATING STATE

We can now leverage the structure of the graph $G(x)$ to obtain the number of distinct bounds on terminating state $x \in \mathcal{X}$ after m samples and get

Theorem A.6 (Expected number of distinct bounds on the reward of a terminating state). *If $Q(m)$ is the number of distinct bounds on any given terminal state x after m uniformly sampled trajectories, then*

$$\mathbb{E}[Q(m)] = \alpha\beta \left(1 - 2 \left(1 - \frac{1}{|\mathcal{T}|} \right)^m + \left(1 - \frac{2}{|\mathcal{T}|} \right)^m \right) \quad (4)$$

Note that this is true for any terminating state x . Hence, every terminating state has the same expected number of distinct bounds, which grows with m , the number of uniformly collected trajectories.

Proof. First, note that there are $\alpha\beta$ edges in $\mathcal{E}(x)$, as each trajectory of the λ trajectories respecting Definition 4.3 can be paired with any of its β compatible trajectories. Since there are $(K+1)$ parents of a given terminating state $x \in \mathcal{X}$, we get $\alpha\beta$ compatible pairs, and thus, $\alpha\beta$ edges in $G(x)$.

Now, for an edge $e_i := (\tau_i, \tau_j) \in \mathcal{E}(x)$, what is the probability that τ_i and τ_j appear at least once in the m samples? Alternatively, one can frame this question as “what is the probability that e_i appears in the induced subgraph $G[W]$ ”, where W is set of trajectories that were sampled.

Let $E_{\tau_i} := \tau_i$ is not in the m samples. Then, using the inclusion-exclusion principle, the probability that edge (τ_i, τ_j) is *not* present in the sample is

$$P(e_i \notin G[W]) = P(E_{\tau_i} \cup E_{\tau_j}) = P(E_{\tau_i}) + P(E_{\tau_j}) - P(E_{\tau_i} \cap E_{\tau_j}).$$

Since we assume the m trajectories are sampled uniformly, we know that $P(E_{\tau_i}) = (1 - 1/|\mathcal{T}|)^m$, $P(E_{\tau_j}) = (1 - 1/|\mathcal{T}|)^m$ and $P(E_{\tau_i} \cap E_{\tau_j}) = (1 - 2/|\mathcal{T}|)^m$. This follows from the fact that for E_{τ_i} to occur, any trajectory except τ_i can be sampled. Therefore, the probability that both appear at least once is the complement:

$$\mathbb{P}(e_i \in G[W]) = P(\neg(E_{\tau_i} \cup E_{\tau_j})) = 1 - 2 \left(1 - \frac{1}{|\mathcal{T}|} \right)^m + \left(1 - \frac{2}{|\mathcal{T}|} \right)^m.$$

Let $Q(m)$ be the number of edges in $G[W]$ and let $\mathbb{1}[e \in G[W]]$ be the indicator function for the inclusion of edge e in the $G[W]$. By linearity of expectation, then we have for arbitrary x the following number of distinct bounds:

$$\begin{aligned}\mathbb{E}[Q(m)] &= \sum_{e \in E} \mathbb{E}[\mathbb{1}[e \in G[W]]] \\ &= \sum_{e \in E} 1 - 2 \left(1 - \frac{1}{|\mathcal{T}|}\right)^m + \left(1 - \frac{2}{|\mathcal{T}|}\right)^m \\ &= \alpha\beta \left(1 - 2 \left(1 - \frac{1}{|\mathcal{T}|}\right)^m + \left(1 - \frac{2}{|\mathcal{T}|}\right)^m\right)\end{aligned}$$

□

A.1.4. ASYMPTOTIC LOWER BOUND

We first lower bound α and β .

Lemma A.7 (Asymptotic lower bound for α). *Let α be as in Proposition A.4, then*

$$\alpha \in \Omega(N(K+1)!).$$

Proof. We have

$$\begin{aligned}\alpha &= (K+1)!(N-K-1) \\ &\geq (K+1)! \left(\frac{N}{2} - 1\right) \quad (K \leq N/2)\end{aligned}$$

Then, if $N \geq 4$, we get that

$$\alpha \geq \frac{N}{4}(K+1)!$$

As such, for $N \geq 4$ and $c = 1/4$, we find that $\alpha \in \Omega(N(K+1)!)$. □

Lemma A.8 (Asymptotic lower bound for β). *Let β be as in Proposition A.5, then*

$$\beta \in \Omega((N-K)^K).$$

Proof. Then,

$$\begin{aligned}\beta &= \prod_{i=0}^{K-1} (N-i) - (K+1)! \\ \beta &\geq (N-K)^K - (K+1)K! \\ \beta &\approx (N-K)^K - (K+1)\sqrt{2\pi K} \left(\frac{K}{e}\right)^K \quad (\text{Stirling})\end{aligned}$$

We can then look at the following limit to determine the dominating term:

$$\lim_{N \rightarrow \infty} \frac{(K+1)\sqrt{2\pi K} \left(\frac{K}{e}\right)^K}{(N-K)^K}$$

Substituting K for $N/2$ from Assumption A.1, we get

$$\begin{aligned}\lim_{N \rightarrow \infty} \frac{((N/2)+1) \sqrt{\pi N} \left(\frac{N/2}{e}\right)^{N/2}}{(N/2)^{N/2}} &= \lim_{N \rightarrow \infty} \frac{((N/2)+1) \sqrt{\pi N} (N/2)^{N/2}}{e^{N/2} (N/2)^{N/2}} \\ &= \lim_{N \rightarrow \infty} \frac{((N/2)+1) \sqrt{\pi N}}{e^{N/2}}.\end{aligned}$$

Since $((N/2) + 1)\sqrt{\pi N}$ is a polynomial and $e^{N/2}$ is an exponential, then the limit goes to 0 and N grows and thus $(N - K)^K$ dominates $(K + 1)!$ as N grows.

Following this, we can deduce $\beta \in \Omega((N - K)^K)$. \square

We can then simplify the probability to make the equation more concise and readable.

Proposition A.9. *If $|\mathcal{T}|$ is large, then the probability term $\left(1 - 2\left(1 - \frac{1}{|\mathcal{T}|}\right)^m + \left(1 - \frac{2}{|\mathcal{T}|}\right)^m\right) \in \Omega\left(\left(1 - e^{-\frac{m}{N^{K+1}}}\right)^2\right)$*

Proof. Let $y = \left(1 - \frac{1}{|\mathcal{T}|}\right)^m$, then

$$\begin{aligned} y &= \left(1 - \frac{1}{|\mathcal{T}|}\right)^m \\ \ln y &= n \ln \left(1 - \frac{1}{|\mathcal{T}|}\right) \\ \ln y &= n \left(-\frac{1}{|\mathcal{T}|} - \frac{\left(\frac{1}{|\mathcal{T}|}\right)^2}{2} - \dots\right) \quad (\text{Maclaurin Series}) \\ \ln y &\approx n \left(-\frac{1}{|\mathcal{T}|}\right) \quad (|\mathcal{T}| \text{ is large } (\in O(N^{K+1}))) \\ y &\approx e^{-\frac{m}{|\mathcal{T}|}}. \end{aligned} \tag{5}$$

Thus, we can simplify the probability term with this approximation:

$$\begin{aligned} \left(1 - 2\left(1 - \frac{1}{|\mathcal{T}|}\right)^m + \left(1 - \frac{2}{|\mathcal{T}|}\right)^m\right) &\approx 1 - 2y + y^2 \\ &= (y - 1)^2 \\ &= (1 - y)^2 \\ &= (1 - e^{-\frac{m}{|\mathcal{T}|}})^2 \\ &\geq \left(1 - e^{-\frac{m}{N^{K+1}}}\right)^2 \quad (\text{Lemma A.2}). \end{aligned} \tag{6}$$

Therefore, $\left(1 - 2\left(1 - \frac{1}{|\mathcal{T}|}\right)^m + \left(1 - \frac{2}{|\mathcal{T}|}\right)^m\right) \in \Omega\left(\left(1 - e^{-\frac{m}{N^{K+1}}}\right)^2\right)$. \square

Since $|\mathcal{T}| \in O(N^{K+1})$ (Lemma A.2), it is fair to assume $|\mathcal{T}|$ is large and thus Proposition A.9 generally holds. Then, combining Propositions A.7, A.8 and A.9, we get Theorem 4.5.

Proof.

$$\begin{aligned} \mathbb{E}[Q(m)] &= \alpha\beta \left(1 - 2\left(1 - \frac{1}{|\mathcal{T}|}\right)^m + \left(1 - \frac{2}{|\mathcal{T}|}\right)^m\right) \\ &= \Omega(N(K+1)!) \cdot \Omega((N-K)^K) \cdot \Omega\left(\left(1 - e^{-\frac{m}{N^{K+1}}}\right)^2\right) \\ &= \Omega\left(N^{K+1}(K+1)! \left(1 - \frac{K}{N}\right)^K \left(1 - e^{-\frac{m}{N^{K+1}}}\right)^2\right) \\ &= \Omega\left(N^C C! \left(1 - \frac{C-1}{N}\right)^{C-1} \left(1 - e^{-\frac{m}{N^C}}\right)^2\right) \end{aligned} \tag{7}$$

\square

A.2. Proof of Theorem 4.6

To prove Theorem 4.6, we must quantify the total pairwise dependence between edges in the graph $G(x)$.

Definition A.10 (Total pairwise dependence between edges). Given a graph $G(x) = (\mathcal{V}, \mathcal{E}(x))$, if $e_i, e_j \in \mathcal{E}(x)$, then $e_i \sim e_j$ denotes that e_i and e_j share a common vertex. Denote A_i the event that e_i has been sampled by the trajectory sampling policy, then the total pairwise dependency is

$$\nu = \sum_{(i,j): e_i \sim e_j} P(A_i \cap A_j)$$

We start by counting the number of edges in $G(x)$ that share a common vertex in order to index the sum. Specifically, there are two types of edges sharing a vertex. We detail and count the number of edges for each type below.

A.2.1. TYPE 1: SINGLE PARENT PAIRS OF EDGES

For a given x and one of its parent $p_{x,a}$, then we previously established that λ trajectories pass through $p_{x,a}$ without terminating in x . Now, each of the β compatible trajectories forms an edge with the λ previous trajectories. As such, taking any two trajectories for the λ parent trajectories and taking one trajectory from the β compatible trajectories produces a pair of edges with a shared vertex (the chosen compatible trajectory). Similarly, taking two trajectories in the β compatible trajectories and one in the λ parent trajectories also produces two edges with shared vertex. Figure 6 illustrates a small example of trajectories and the edges linking them. We can then deduce the following lemma.

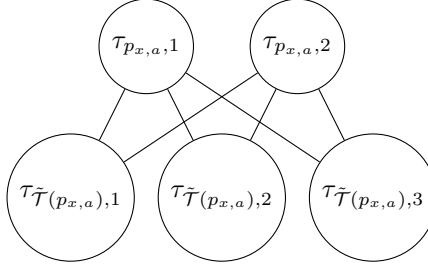


Figure 6. Any pair of trajectories $\tau_{p_{x,a},1}$ and $\tau_{p_{x,a},2}$ passing through a parent $p_{x,a}$ have edges that share common vertices. These vertices are trajectories $\tau_{\tilde{\mathcal{T}}(p_{x,a}),i} \in \tilde{\mathcal{T}}(p_{x,a})$.

Lemma A.11. *There are $(K+1) \left[\binom{\lambda}{2} \beta + \binom{\beta}{2} \lambda \right]$ Type 1 pairs of edges sharing a vertex.*

Proof. Let $p_{x,a}$ be a parent of x , then $|\mathcal{T}(p_{x,a})| = \lambda$. There are $\binom{\lambda}{2}$ pairs of trajectories in $\mathcal{T}(p_{x,a})$ that can be coupled with any one of their compatible trajectories in $\tilde{\mathcal{T}}(p_{x,a})$. Applying the same reasoning for the pairs in $\tilde{\mathcal{T}}(p_{x,a})$, and remarking there are $(K+1)$ such parents yields our result. \square

A.2.2. TYPE 2: EXTRA-PARENT PAIRS

Now, we start with the observation that for two parents of x , $p_{x,a}$ and $p_{x,b}$, their sets of compatible trajectories is not mutually exclusive, i.e. $\tilde{\mathcal{T}}(p_{x,a}) \cap \tilde{\mathcal{T}}(p_{x,b}) \neq \emptyset$. As such, any edge with a vertex in $\tilde{\mathcal{T}}(p_{x,a}) \cap \tilde{\mathcal{T}}(p_{x,b})$ can be coupled with trajectories in $\mathcal{T}_{p_{x,a}}$ and $\mathcal{T}_{p_{x,b}}$. As such, these are also edges with a shared vertex. Figure 7 illustrates an example.

To establish our result, we first count how many vertices are in the intersection.

Lemma A.12. *Let $\phi := |\tilde{\mathcal{T}}(p_{x,a}) \cap \tilde{\mathcal{T}}(p_{x,b})|$, then*

$$\phi = 2 \prod_{i=0}^K (N - i) - K! ((N - K)(K - 1) - 2)$$

Proof. To quantify ϕ , we show our reasoning as a sequence of steps. Fix x and take $p_{x,a} := x \setminus a$ and $p_{x,b} := x \setminus b$, two parents of x . Notice that $|p_{x,a} \cap p_{x,b}| = K - 1$. A trajectory can be compatible with both $p_{x,a}$ and $p_{x,b}$ if it follows the following steps:

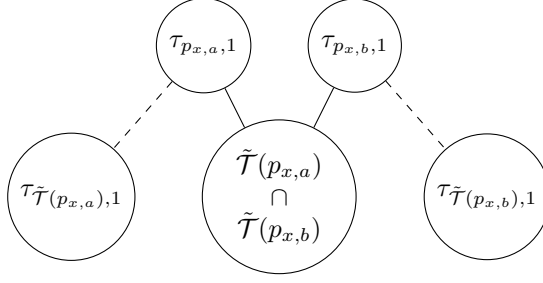


Figure 7. Any pair of trajectories $\tau_{p_{x,a},1}$ and $\tau_{p_{x,b},1}$ passing through different parents of x , have edges that share common vertices. These vertices are trajectories in $\tilde{\mathcal{T}}(p_{x,a}) \cap \tilde{\mathcal{T}}(p_{x,b})$.

1. Pick any permutation of $L_1 \leq K - 2$ elements out of the $K - 1$ common elements between $p_{x,a}$ and $p_{x,b}$.
 - $L \leq K - 2$ since we need to preserve space for a and b to be added.
 - $|s| = L_1$
 - $s \subset (p_{x,a} \cap p_{x,b})$
 - That is $(K - 1)!/(K - 1 - L_1)!$ permutations.
2. Pick either a or b to add to the set. w.l.o.g. Let's assume a was picked. Switch a, b and $p_{x,a}, p_{x,b}$ if b is picked.
 - $|s| = L_1 + 1$
 - This trajectory is now compatible with $p_{x,a}$
 - $s \subset p_{x,b}, s \not\subset p_{x,a}$
 - Since there are two choices (a or b) here, we will multiply by 2 the number of trajectories down the line.
3. Add $L_2 \leq K - L_1 - 2$ elements out of $K - L_1 - 1$ remaining elements in $p_{x,b}$
 - $K - L_1 - 2 = K - (L_1 + 1) - 1$, so that there is still space to add b to the set.
 - $|s| = L_1 + 1 + L_2$
 - $s \subset p_{x,b}$
 - That is $(K - L_1 - 1)!/(K - L_1 - 1 - L_2)!$ permutations.
4. Add b to the set.
 - $|s| = L_1 + L_2 + 2$
 - $s \not\subset p_{x,b}$
 - This trajectory now gives a bound via $p_{x,b} \cup b$
5. Add any element until $|s| = K + 1$.
 - That is $(N - L_1 - L_2 - 2)!/(N - K - 1)!$ permutations, that must be multiplied.
6. We need to subtract sub-trajectories passing through other parents of x to avoid double counting in the set of Type 1 edges. This is because for a parent $p_{x,a}$, $\mathcal{T}(p_{x,a}) \subset \tilde{\mathcal{T}}(p_{x,a})$ for any other parent $p_{x,..}$. Therefore, we must subtract the following number of trajectories:
 - There are $L_1 + L_2 + 2$ elements in x that have already been taken.
 - Choosing $K - L_1 - L_2 - 2$ elements in the set of $K + 1 - L_1 - L_2 - 2$ non-chosen elements in x will result in a parent of x in the trajectory.
 - $\frac{(K - L_1 - L_2 - 1)!}{(K - L_1 - L_2 - 1 - K + L_1 + L_2 + 2)!} = (K - L_1 - L_2 - 1)!$ sub-trajectories leading to parents of x from s .
 - Once a parent is reached, $|s| = K$. Then $N - K$ remaining choices to terminate trajectory.
 - $(N - K)(K - L_1 - L_2 - 1)!$ trajectories to subtract.

So, summing across L_1 and L_2 , and subtracting the trajectories leading to other parents of x , we get:

$$\begin{aligned} \phi &= 2 \sum_{L_1=0}^{K-2} \frac{(K-1)!}{(K-1-L_1)!} \\ &\quad \sum_{L_2=0}^{K-L_1-2} \frac{(K-L_1-1)!}{(K-L_1-L_2-1)!} \left[\frac{(N-L_1-L_2-2)!}{(N-K-1)!} - (N-K)(K-L_1-L_2-1)! \right] \\ &= 2(K-1)! \sum_{L_1=0}^{K-2} \sum_{L_2=0}^{K-L_1-2} \left[\binom{N-L_1-L_2-2}{K-L_1-L_2-1} - (N-K) \right]. \end{aligned} \quad (8)$$

We can simplify ϕ further by once again making use of the HSI and sum identities and get

$$\begin{aligned} \phi &= 2(K-1)! \sum_{L_1=0}^{K-2} \sum_{L_2=0}^{K-L_1-2} \left[\binom{N-L_1-L_2-2}{K-L_1-L_2-1} - (N-K) \right] \\ &= 2(K-1)! \sum_{L_1=0}^{K-2} \left[\binom{N-L_1-1}{K-L_1-1} - (K-L_1-1)(N-K) - 1 \right] \quad (\text{HSI}) \\ &= 2(K-1)! \left[\binom{N}{K-1} - 1 - \frac{(N-K)K(K-1)}{2} - (K-1) \right] \quad (\text{HSI and sum identities}) \\ &= 2(K-1)! \left[\binom{N}{K-1} - \frac{(N-K)K(K-1)}{2} - K \right] \\ &= 2 \prod_{i=0}^K (N-i) - K! ((N-K)(K-1) - 2) \end{aligned} \quad (9)$$

□

We can now state the number of Type 2 pairs of edges.

Lemma A.13. *There are $\binom{K+1}{2} \lambda^2 \phi$ Type 2 pairs of edges sharing a vertex.*

Proof. Let $p_{x,a}$ and $p_{x,b}$ be two parents of x . One can choose any trajectory in $\mathcal{T}(p_{x,a})$, another in $\mathcal{T}(p_{x,b})$ and lastly a third in $\tilde{\mathcal{T}}(p_{x,a}) \cap \tilde{\mathcal{T}}(p_{x,b})$. Recalling $|\mathcal{T}(p_{x, \cdot})| = \lambda$, then there are $\lambda^2 \phi$ pairs of edges with a shared vertex by pair of parents. Since there are $\binom{K+1}{2}$ pairs of parents, we get our result. □

A.2.3. PROBABILITY OF SAMPLING TWO EDGES WITH A COMMON VERTEX

It remains to properly quantify $P(A_i \cap A_j)$. The following lemma gives our result.

Lemma A.14. *Let $P(A_i \cap A_j)$ be the probability of sampling two edges in $G(x)$ such that one vertex is shared by both edges. Then*

$$P(A_i \cap A_j) \approx (1 - e^{-\frac{m}{|\mathcal{T}|}})^3.$$

Proof. Now, $P(A_i \cap A_j)$ can be thought of as the probability of sampling 3 vertices (e.g. (τ_i, τ_j, τ_k) if $e_i = (\tau_i, \tau_k)$ and $e_j = (\tau_j, \tau_k)$). Following Assumption 4.2, the probability of sampling any specific trajectory in m attempts is $(1/|\mathcal{T}|)^m$. Let E_i be the event that $\tau_i \in \mathcal{V}$ has not been sampled after m trajectories, then by the inclusion-exclusion principle we have

$$\begin{aligned} P(E_i \cup E_j \cup E_k) &= P(E_i) + P(E_j) + P(E_k) - P(E_i \cap E_j) - P(E_i \cap E_k) - P(E_j \cap E_k) + P(E_i \cap E_j \cap E_k) \\ &= 3 \left(1 - \frac{1}{|\mathcal{T}|} \right)^m - 3 \left(1 - \frac{2}{|\mathcal{T}|} \right)^m + \left(1 - \frac{3}{|\mathcal{T}|} \right)^m \\ &= 3 \left(1 - \frac{1}{|\mathcal{T}|} \right)^m - 3 \left(1 - \frac{2}{|\mathcal{T}|} \right)^m + \left(1 - \frac{3}{|\mathcal{T}|} \right)^m \end{aligned} \quad (10)$$

Therefore, the probability of all three vertices occurring (coinciding with the probability of two edges with a shared vertex being sampled)

$$\begin{aligned} P(A_i \cap A_j) &= P(\neg(E_i \cup E_j \cup E_k)) \\ &= 1 - \left(3 \left(1 - \frac{1}{|\mathcal{T}|} \right)^m - 3 \left(1 - \frac{2}{|\mathcal{T}|} \right)^m + \left(1 - \frac{3}{|\mathcal{T}|} \right)^m \right). \end{aligned} \quad (11)$$

Using the simplification trick shown in Equation 5, we get

$$\begin{aligned} P(A_i \cap A_j) &\approx 1 - 3y + 3y^2 - y^3 \\ &= (1 - y)^3 \\ &= (1 - e^{-\frac{m}{|\mathcal{T}|}})^3. \end{aligned} \quad (12)$$

□

We are now ready to quantify the total pairwise dependency in $G(x)$ after m samples are taken.

Lemma A.15 (Total pairwise dependency). *Let $\nu(m)$ denote the total pairwise dependency in the graph after m samples, then*

$$\nu(m) = (K+1) (\lambda(\lambda-1)\beta + \beta(\beta-1)\lambda + K\lambda^2\phi) \left(1 - e^{-\frac{m}{|\mathcal{T}|}}\right)^3$$

Proof. We directly combine Lemmas A.11, A.13 and A.14 and simplify. Note that the total number of edges with a shared vertex is $2 \left((K+1) \left[\binom{\lambda}{2} \beta + \binom{\beta}{2} \lambda \right] + \binom{K+1}{2} \lambda^2 \phi \right)$, as the total pairwise dependency requires us to account for both (e_i, e_j) and (e_j, e_i) when summing and so

$$\begin{aligned} \nu(m) &= \sum_{(e_i, e_j): e_i \sim e_j} P(A_i \cap A_j) \\ &= 2 \left((K+1) \left[\binom{\lambda}{2} \beta + \binom{\beta}{2} \lambda \right] + \binom{K+1}{2} \lambda^2 \phi \right) \left(1 - e^{-\frac{m}{|\mathcal{T}|}}\right)^3 \\ &= (K+1) (\lambda(\lambda-1)\beta + \beta(\beta-1)\lambda + K\lambda^2\phi) \left(1 - e^{-\frac{m}{|\mathcal{T}|}}\right)^3 \end{aligned} \quad (13)$$

□

A.2.4. PROOF OF MAIN RESULT

Combining Lemmas A.15 and Theorem A.6, we leverage Janson's Inequalities (Bollobás, 1988; Janson et al., 1988), yielding the following result.

Theorem A.16. *Let $Q(m)$ be the number of bounds on x after m trajectories, then*

$$\mathbb{P}(Q(m) > 0) \geq 1 - \min \left\{ e^{-\mathbb{E}[Q(m)] + \nu(m)/2}, e^{-\mathbb{E}[Q(m)]^2 / (\nu(m) + \mathbb{E}[Q(m)])} \right\}$$

,

where $\mathbb{E}[Q(m)]$ and $\nu(m)$ are as in Theorem A.6 and Lemma A.15 respectively.

A.2.5. ASYMPTOTIC LOWER BOUND FOR THEOREM A.16

To produce an asymptotic lower bound for $P(Q(m) > 0)$, we must investigate when the exponents in the min are the least negative. This means $\mathbb{E}[Q(m)]$ should be small and $\nu(m)$ should be large. As we already have an asymptotic lower bound on $\mathbb{E}[Q(m)]$, we only need an asymptotic upper-bound on $\nu(m)$.

For this, we first need asymptotic upper bounds on λ, β and ϕ .

Lemma A.17 (Asymptotic upper bound on λ). *Let λ be the number of trajectories passing through a parent $p_{x, \cdot}$, then $\lambda \in O(NK!)$.*

Proof.

$$\begin{aligned}
 \lambda &= K!(N - K - 1) \\
 &\leq K!(N - K) \\
 &\leq K!N \\
 \implies \lambda &\in O(NK!)
 \end{aligned} \tag{14}$$

□

Lemma A.18 (Asymptotic upper bound on β). *Let β be the number of compatible trajectories for a parent $p_{x, \cdot}$, then $\beta \in O(N^K)$.*

Proof.

$$\begin{aligned}
 \beta &= \prod_{i=0}^{K-1} (N - i) - (K + 1)! \\
 &\leq \prod_{i=0}^{K-1} (N - i) \\
 &\leq N^K \\
 \implies \beta &\in O(N^K)
 \end{aligned} \tag{15}$$

□

Lemma A.19 (Asymptotic upper bound for ϕ). *Let $\phi := |\tilde{\mathcal{T}}(p_{x,a}) \cap \tilde{\mathcal{T}}(p_{x,a})|$, then $\phi \in O(N^{K+1})$.*

Proof.

$$\phi = 2 \prod_{i=0}^K (N - i) - K!((N - K)(K - 1) - 2) \leq N^{K+1} \implies \phi \in O(N^{K+1})$$

□

Lemma A.20 (Asymptotic lower bound on total pairwise dependence). *Let $\nu(m)$ be the total pairwise dependence between edges in $G(x)$, then $\nu(N, K, m) \in O(KK!N^{2K+1}) \left(1 - e^{-\frac{m}{|\mathcal{T}|}}\right)^3$.*

Proof.

$$\begin{aligned}
 \nu(m) &= (K + 1) (\lambda(\lambda - 1)\beta + \beta(\beta - 1)\lambda + K\lambda^2\phi) \left(1 - e^{-\frac{m}{|\mathcal{T}|}}\right)^3 \\
 &= (O(K) \cdot O(NK!) \cdot O(NK!) \cdot O(N^K)) \left(1 - e^{-\frac{m}{|\mathcal{T}|}}\right)^3 \\
 &\quad + (O(K) \cdot O(N^K) \cdot O(N^K) \cdot O(NK!)) \left(1 - e^{-\frac{m}{|\mathcal{T}|}}\right)^3 \\
 &\quad + (O(K) \cdot O(K) \cdot O(NK) \cdot O(NK) \cdot O(N^{K+1})) \left(1 - e^{-\frac{m}{|\mathcal{T}|}}\right)^3 \\
 &= O(K(K!)^2 N^{K+2}) \left(1 - e^{-\frac{m}{|\mathcal{T}|}}\right)^3 \\
 &\quad + O(KK!N^{2K+1}) \left(1 - e^{-\frac{m}{|\mathcal{T}|}}\right)^3 \\
 &\quad + O(K^4 N^{K+3}) \left(1 - e^{-\frac{m}{|\mathcal{T}|}}\right)^3
 \end{aligned} \tag{16}$$

We then show $O(KK!N^{2K+1})$ dominates the other terms as N grows.

$$\begin{aligned}
\lim_{N \rightarrow \infty} \frac{K(K!)^2 N^{K+2}}{KK! N^{2K+1}} &= \lim_{N \rightarrow \infty} \frac{K(K!)^2 N^{K+2}}{KK! N^K N^{K+2} N^{K-1}} \\
&= \lim_{N \rightarrow \infty} \frac{K!}{N^{K-1}} \\
&\approx \lim_{N \rightarrow \infty} \frac{\sqrt{2\pi K} \left(\frac{K}{e}\right)^K}{N^{K-1}} \quad (\text{Stirling}) \\
&= \lim_{N \rightarrow \infty} \frac{\sqrt{\pi} N^{N/2}}{(2e)^{N/2} N^{N/2-1}} \quad (K \leq N/2) \\
&= \lim_{N \rightarrow \infty} \frac{\sqrt{\pi} N^{3/2}}{(2e)^{N/2}} \\
&= 0
\end{aligned} \tag{17}$$

since the denominator (exponential growth) grows much faster than the numerator (polynomial growth). This implies $O(KK!N^{2K+1})$ dominates $O(K(K!)^2N^{K+2})$. Applying the same reasoning for $O(K^4N^{K+3})$ we get

$$\begin{aligned}
\lim_{N \rightarrow \infty} \frac{K^4 N^{K+3}}{K K! N^{2K+1}} &= \lim_{N \rightarrow \infty} \frac{K^3 N^{K+3}}{K! N^{K+3} N^{K-2}} \\
&= \lim_{N \rightarrow \infty} \frac{K^3}{K! N^{K-2}} \\
&= 0,
\end{aligned} \tag{18}$$

since the numerator is a polynomial of K and the denominator grows factorially in K (at least). This implies $O(KK!N^{2K+1})$ dominates $O(K^4N^{K+3})$. Therefore,

$$\nu(N, K, m) \in O\left(KK!N^{2K+1}\right) \left(1 - e^{-\frac{m}{|T|}}\right)^3. \quad (19)$$

We can now investigate the relationship between the asymptotic bounds for $\mathbb{E}[Q(m)]$ and $\nu(m)$.

$$\begin{aligned}
\frac{\mathbb{E}[Q(m)]}{\nu(m)} &= \frac{N(K+1)!(N-K)^K \left(1 - e^{-\frac{m}{\lceil T \rceil}}\right)^2}{KK!N^{2K+1} \left(1 - e^{-\frac{m}{\lceil T \rceil}}\right)^3} \\
&= \frac{(K+1)(N-K)^K}{KN^{2K} \left(1 - e^{-\frac{m}{\lceil T \rceil}}\right)} \\
&= \frac{\left(\frac{N}{2}+1\right) \left(\frac{N}{2}\right)^{N/2}}{\frac{N}{2}N^N \left(1 - e^{-\frac{m}{\lceil T \rceil}}\right)} \quad (K \leq N/2) \\
&= \frac{\left(\frac{N}{2}+1\right)}{2^{N/2} \frac{N}{2}N^{N/2} \left(1 - e^{-\frac{m}{\lceil T \rceil}}\right)} \\
&= \frac{1}{2^{N/2}N^{N/2} \left(1 - e^{-\frac{m}{\lceil T \rceil}}\right)} + \frac{1}{2^{N/2-1}N^{N/2+1} \left(1 - e^{-\frac{m}{\lceil T \rceil}}\right)}
\end{aligned} \tag{20}$$

As such, we find that the upper bound for $\nu(m)$ dominates the lower bound for $\mathbb{E}[Q(m)]$ as N grows. Since that is the case, it is a known result that the bound $1 - e^{-\mathbb{E}[Q(m)] + \nu(m)/2}$ is vacuous. Thus, we investigate only the asymptotic lower bound of the term $\mathbb{E}[Q(m)]^2/(\nu(m) + \mathbb{E}[Q(m)])$.

Lemma A.21 (Asymptotic lower bound for exponent in Janson's inequalities). *Let $\Lambda(m)$ be the exponent in Janson's second inequality, then $\Lambda(m) \in \Omega\left(NK! \left(1 - \frac{K}{N}\right)^{2K} \left(1 - e^{-\frac{m}{N^{K+1}}}\right)\right)$*

Proof.

$$\begin{aligned}
 \frac{\mathbb{E}[Q(m)]^2}{\nu(m) + \mathbb{E}[Q(m)]} &= \frac{\Omega\left(N(K+1)K!(N-K)^K \left(e^{-\frac{m}{N}} - 1\right)^2\right)^2}{O\left(KK!N^{2K+1} \left(1 - e^{-\frac{m}{N}}\right)^3\right)} && (\nu(m) \text{ dominates } \mathbb{E}[Q(m)]) \\
 &= \Omega\left(\frac{\left(N(K+1)K!(N-K)^K \left(e^{-\frac{m}{N}} - 1\right)^2\right)^2}{KK!N^{2K+1} \left(1 - e^{-\frac{m}{N}}\right)^3}\right) \\
 &= \Omega\left(\frac{\left(N(K+1)K!(N-K)^K \left(1 - e^{-\frac{m}{N}}\right)^2\right)^2}{KK!N^{2K+1} \left(1 - e^{-\frac{m}{N}}\right)^3}\right) \\
 &= \Omega\left(\frac{N^2(K+1)^2(K!)^2(N-K)^{2K} \left(1 - e^{-\frac{m}{N}}\right)^4}{KK!N^{2K+1} \left(1 - e^{-\frac{m}{N}}\right)^3}\right) \\
 &= \Omega\left(\frac{(K+1)^2(K-1)!(N-K)^{2K} \left(1 - e^{-\frac{m}{N}}\right)}{N^{2K-1}}\right) \\
 &= \Omega\left(\frac{(K+1)^2(K-1)!N^{2K} \left(1 - \frac{K}{N}\right)^{2K} \left(1 - e^{-\frac{m}{N}}\right)}{N^{2K-1}}\right) \\
 &= \Omega\left((K+1)^2(K-1)!N \left(1 - \frac{K}{N}\right)^{2K} \left(1 - e^{-\frac{m}{N}}\right)\right) \\
 &= \Omega\left(NK! \left(1 - \frac{K}{N}\right)^{2K} \left(1 - e^{-\frac{m}{N}}\right)\right) && ((K+1)^2 \geq (K+1)K) \\
 &= \Omega\left(NK! \left(1 - \frac{K}{N}\right)^{2K} \left(1 - e^{-\frac{m}{N^{K+1}}}\right)\right) && (\text{Lemma A.2})
 \end{aligned} \tag{21}$$

□

The lower bound on the exponent gives the lower bound on the probability and Theorem 4.6 is obtained by combining Lemma A.21 with Theorem A.16.

A.3. Proof of Corollary 4.7

Proof. Let $B_x(m)$ be the event that terminating state $x \in \mathcal{X}$ has a bound after m uniformly collected trajectories and \mathbb{I} be defined as follows:

$$\mathbb{I}_{B_x(m)} = \begin{cases} 1 & \text{if Event } B_x(m) \text{ occurs} \\ 0 & \text{otherwise} \end{cases}$$

We directly apply the definition of expectation with Theorem A.16.

$$\begin{aligned}
 \mathbb{E}[\kappa(m)] &\geq \mathbb{E} \left[\sum_{x \in \mathcal{X}} \mathbb{I}_{B_x(m)} \right] \\
 &= \sum_{x \in \mathcal{X}} \mathbb{E} [\mathbb{I}_{B_x(m)}] \\
 &= \sum_{x \in \mathcal{X}} \mathbb{P}(B_x(m)) \\
 &= \sum_{x \in \mathcal{X}} \mathbb{P}(Q(m) > 0) \\
 &= \binom{N}{C} \mathbb{P}(Q(m) > 0) \\
 &= \binom{N}{C} \mathbb{P}(Q(m) > 0) \quad (\text{Thm. A.16})
 \end{aligned} \tag{22}$$

□

A.4. Proof of Theorem 5.1

Proof. Let $\bar{\mathcal{X}}_{\text{UB}} \subseteq \mathcal{X}$ be the set of observed terminating states (i.e. for which we know the reward) and let $\mathcal{X}_{\text{UB}} := \mathcal{X} \setminus \bar{\mathcal{X}}_{\text{UB}}$ denote the subset of unobserved terminating states. We assume we have an upper bound for every $x \in \mathcal{X}_{\text{UB}}$. Then, given $x \in \mathcal{X}_{\text{UB}}$, we have

$$\begin{aligned}
 \tilde{P}(x) &\geq P(x) \\
 \frac{\text{UB}(x)}{\tilde{Z}} &\geq \frac{R(x)}{Z} \\
 \text{UB}(x) &\geq \frac{R(x)\tilde{Z}}{Z} \\
 &\geq R(x) \frac{Z + \sum_{x' \in \mathcal{X}_{\text{UB}}} \Delta(x')}{Z} \\
 &\geq R(x) \left(1 + \frac{\sum_{x' \in \mathcal{X}_{\text{UB}}} \Delta(x')}{Z} \right) \\
 &= R(x) + R(x) \frac{\sum_{x' \in \mathcal{X}_{\text{UB}}} \Delta(x')}{Z} \\
 &= R(x) + P(x) \sum_{x' \in \mathcal{X}_{\text{UB}}} \Delta(x')
 \end{aligned} \tag{23}$$

which implies

$$\begin{aligned}
 \Delta(x) &\geq P(x) \sum_{x' \in \mathcal{X}_{\text{UB}}} \Delta(x') \\
 &= P(x)\Delta(x) + P(x) \sum_{x' \in \mathcal{X}_{\text{UB}} \setminus \{x\}} \Delta(x') \\
 (1 - P(x))\Delta(x) &\geq P(x) \sum_{x' \in \mathcal{X}_{\text{UB}} \setminus \{x\}} \Delta(x') \\
 \frac{(1 - P(x))}{P(x)} \Delta(x) &\geq \sum_{x' \in \mathcal{X}_{\text{UB}} \setminus \{x\}} \Delta(x')
 \end{aligned} \tag{24}$$

□

B. Experiments on Synthetic Random Graphs

For synthetic instances using random Barabási–Albert (BA) and Erdős–Rényi (ER), we generate graphs with $N = 1000$ vertices. BA-graphs use preferential attachment as a mechanism to distribute the edges, whereas ER-graphs are more random, where each edge has the same probability of occurrence. Thus, the two types of graphs model very different edge distribution (and thus reward distribution). BA-graphs are parameterized by an integer which determines how many neighbors a new node added to the graph should have. The probability of a node being a neighbor is proportional to the degree of this node. We choose 3 as our parameter. For ER-graphs, we choose parameter value 0.005, which is the probability that an edge between two vertices exists. This probability is constant for the entire ER-graph.

These parameters were chosen so as to create relatively small instances with a similar number of edges with different underlying reward distributions. We show the distribution of the edges across instances in Figure 8.

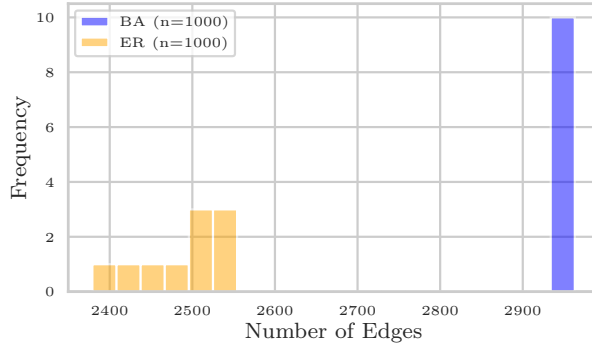


Figure 8. Distribution of the number of edges for the random graph instances.

C. Additional Results

We present here additional results on the tasks presented on the main body of the paper, including $C \in \{5, 10\}$. For every figure, the dashed line, beginning at the circle (●) marker, indicates the approaches are training offline (i.e. no more queries to R are allowed). The diamond (◆) indicates the end of the experiment.

C.1. Random Graphs

Figures 9, 10 and 11 show the full results for the random graphs, including performance metrics (FCS, Loss curves, Top-100 Average Rewards) as well as the number of upper bounds generated by SUBO-GFN.

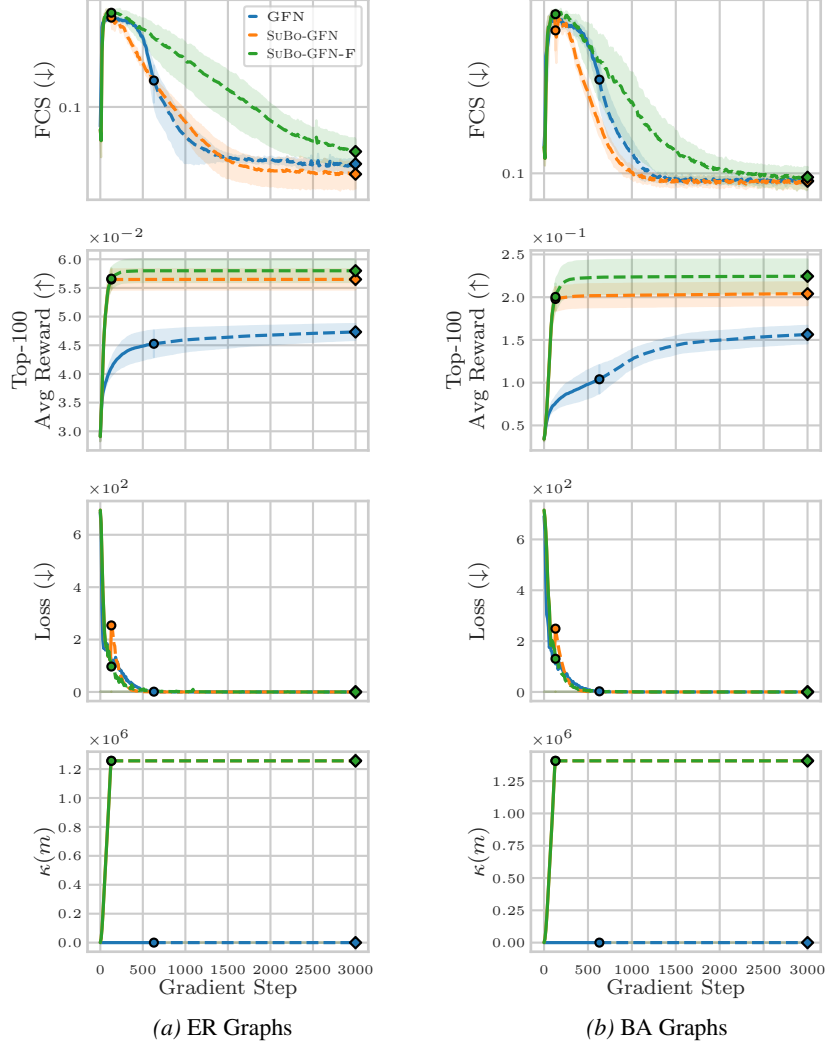


Figure 9. FCS and Top-100 Average Reward of SuBo-GFN and the classical GFN on random graphs with $C = 5$.

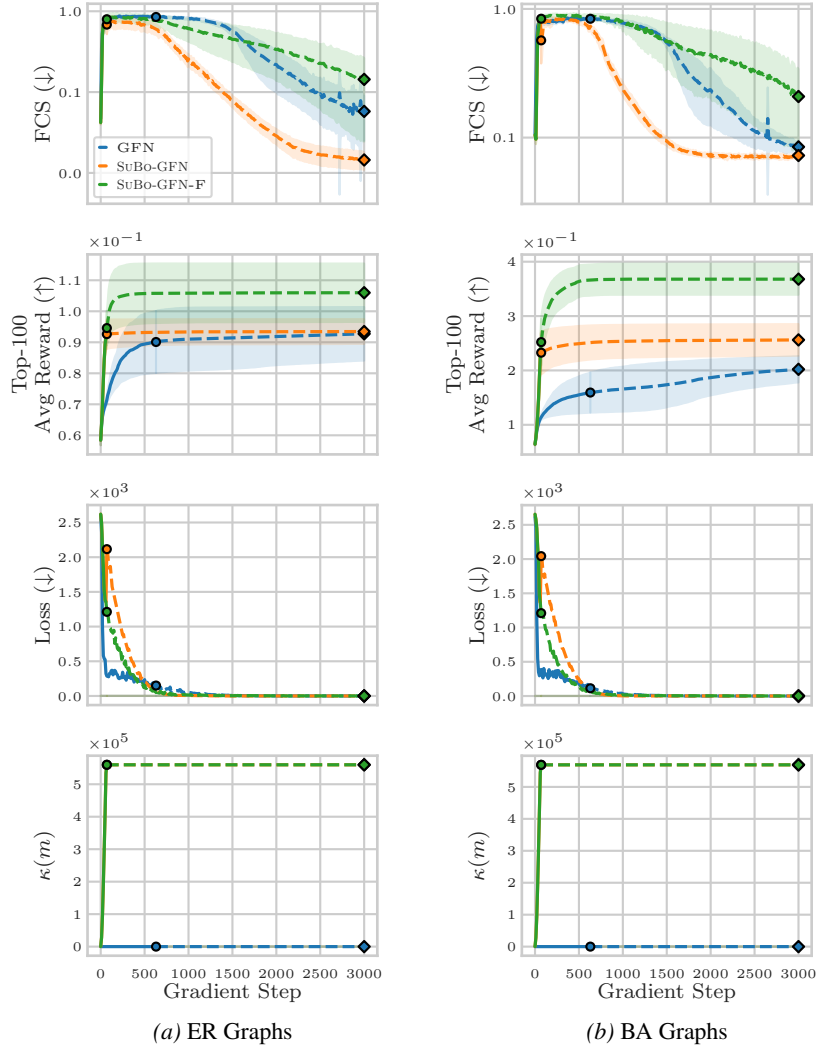


Figure 10. FCS and Top-100 Average Reward of SuBo-GFN and the classical GFN on random graphs with $C = 10$.

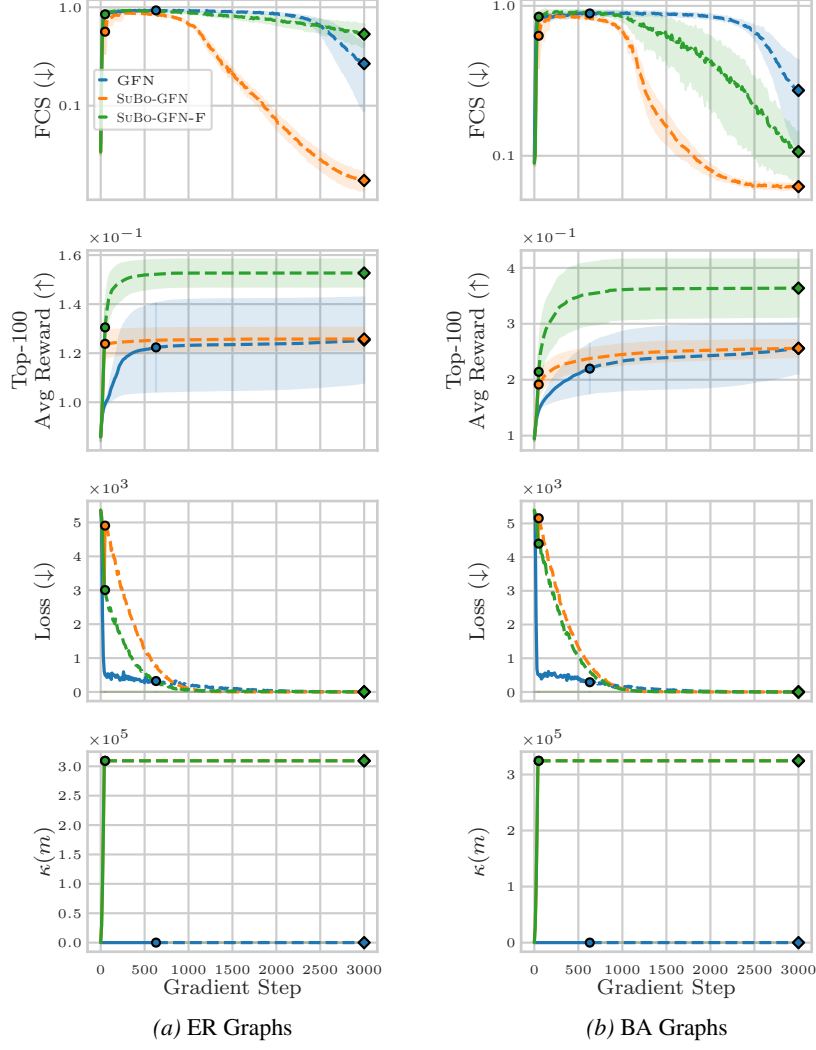


Figure 11. FCS and Top-100 Average Reward of SUBO-GFN and the classical GFN on random graphs with $C = 15$.

Distribution matching and loss We notice that in instances with $C = 5$, the classical GFN is capable of distributing its flow somewhat efficiently, rivalling SUBO-GFN. Across instances and values of C , SUBO-GFN-F is more variable when it comes to FCS and generally struggles to improve it. As C becomes larger, improvements in the loss seems to translate to improvements in the FCS only with SUBO-GFN. That is, classical GFNs improve the loss very fast, but still do not have a small FCS when the loss is small. In contrast, the FCS curves for SUBO-GFN goes down as the loss goes down. This is likely directly due to the sheer amount of data it can train on, thus avoiding overfitting on a restricted set of terminating states and trajectories. This is especially apparent on when the problem instances become larger (as C increases in size), as the loss reduction slows down. As problems become more difficult (i.e. as C grows, we see the classical GFN starting to struggle to reduce the FCS, whereas SUBO-GFN improves it consistently across instances of varying difficulties.

Top-100 Average Rewards In small instances, SUBO-GFN and SUBO-GFN-F significantly outperform classical GFNs. However, there seems to be a trend of the classical GFN catching up to SUBO-GFN in terms of Top-100 Average Reward as C increases. Still, SUBO-GFN(-F) outperforms or rivals the classical GFN in Top-100 Average Reward. This indicates that leveraging bounds, specifically because they are numerous, seems to improve the discovery of high reward states.

Number of bounds We note that SUBO-GFN generates orders of magnitudes more training data than regular GFNs.

C.2. Real-World Graphs

Figures 12, 13 and 14 show the full results for the random graphs, including performance metrics (FCS, Loss curves, Top-100 Average Rewards) as well as the number of upper bounds generated by SuBo-GFN.

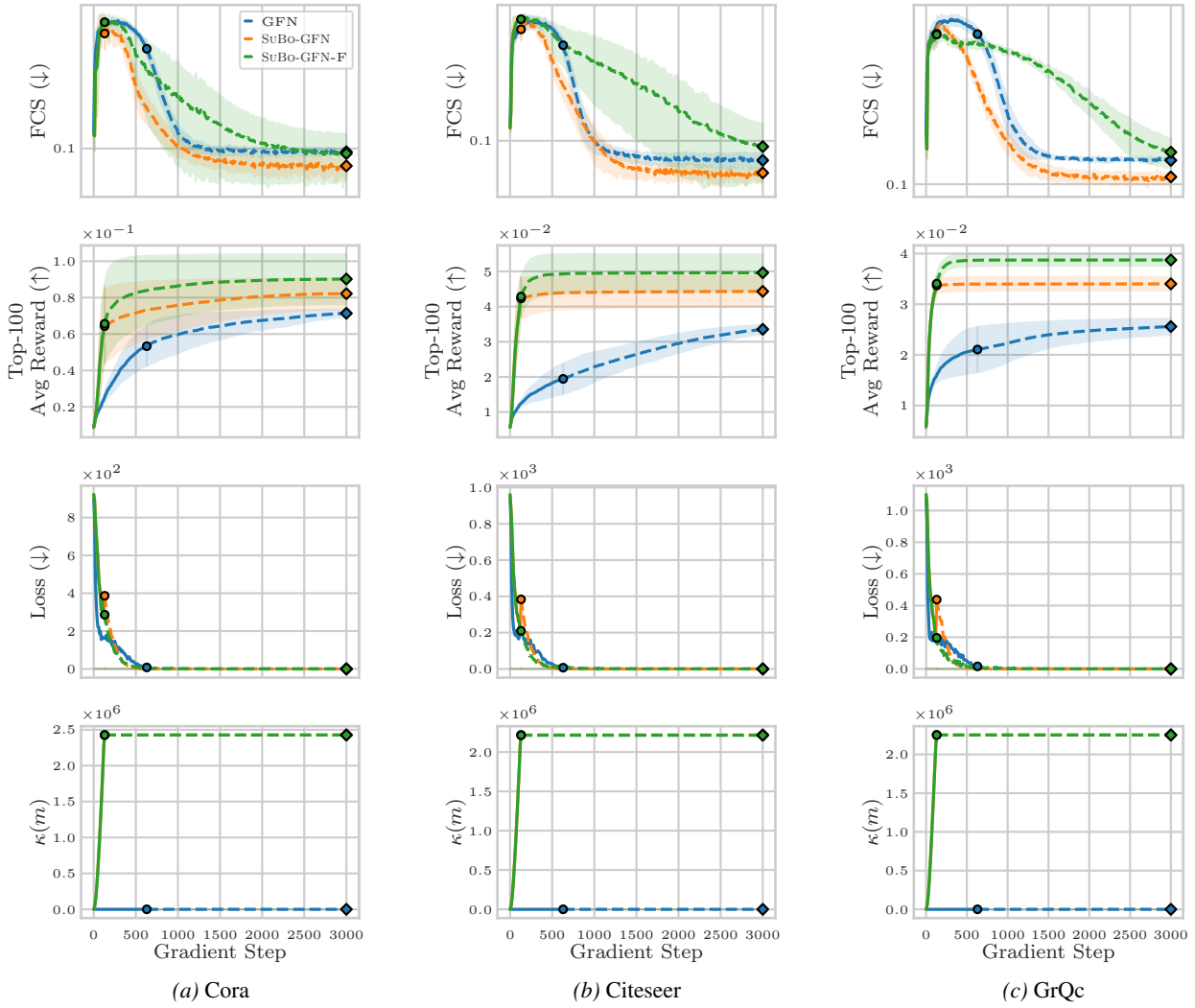


Figure 12. FCS and Top-100 Average Reward of SuBo-GFN and the classical GFN on real-world graphs with $C = 5$.

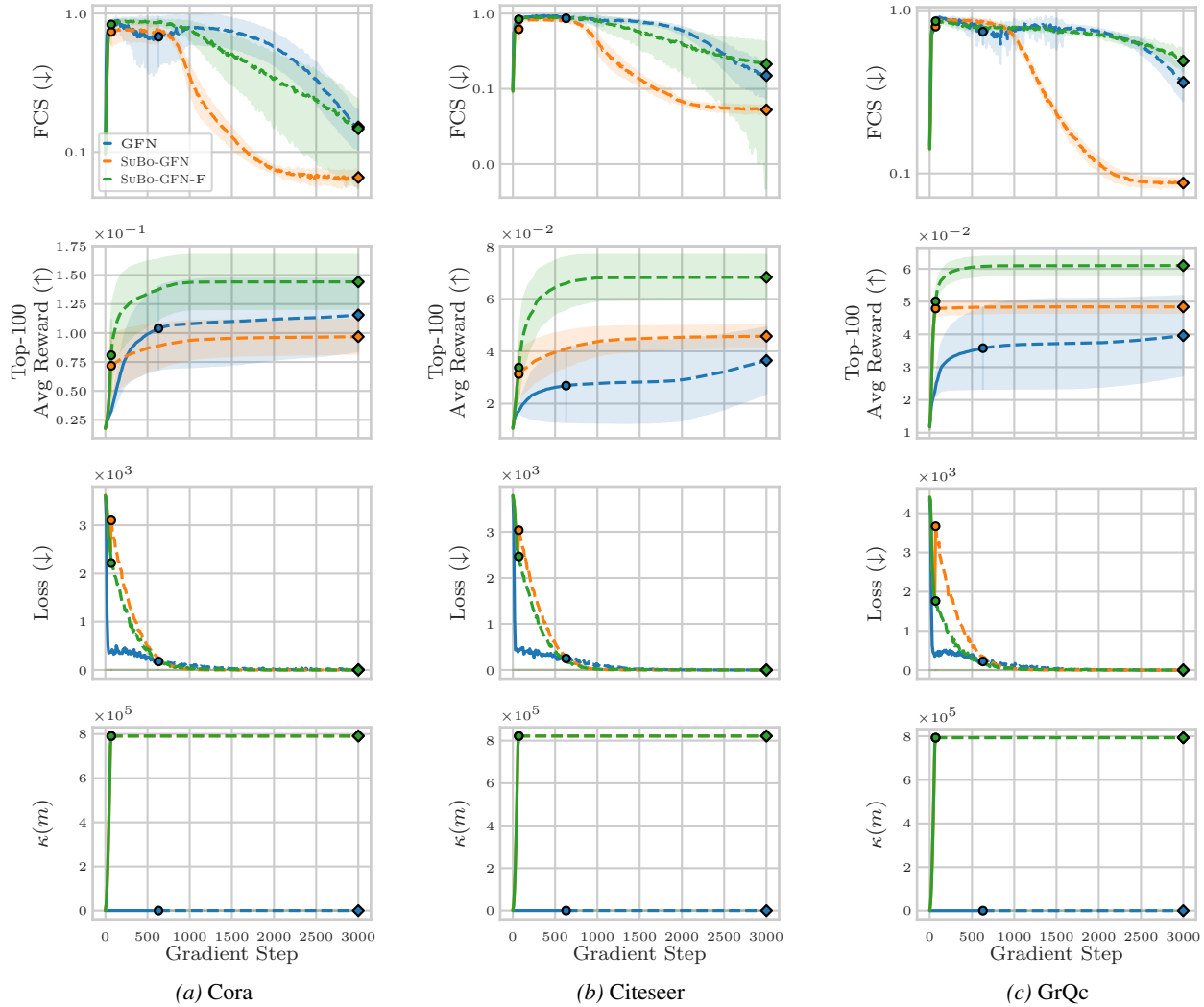


Figure 13. FCS and Top-100 Average Reward of SuBo-GFN and the classical GFN on real-world graphs with $C = 10$.

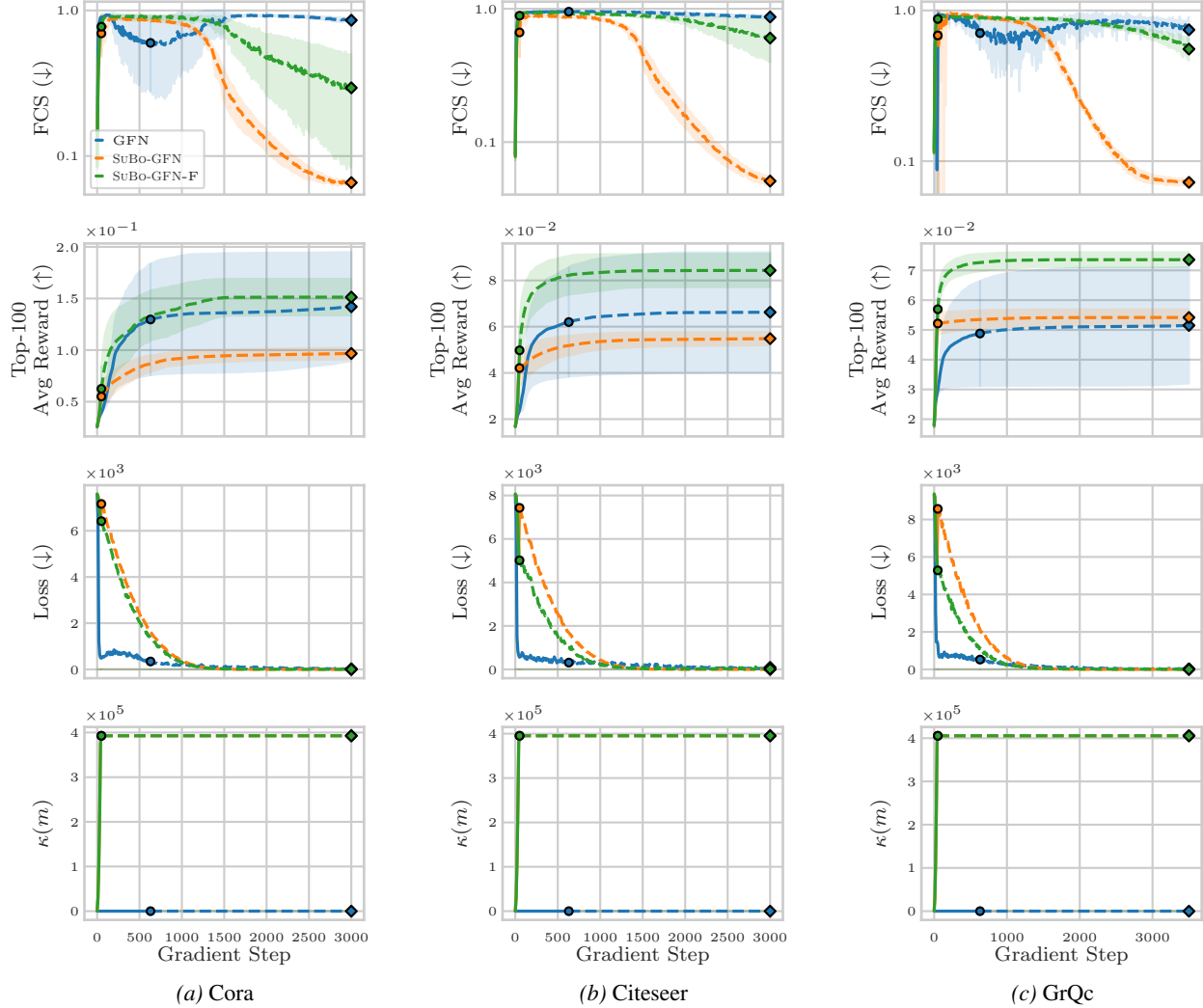


Figure 14. FCS and Top-100 Average Reward of SubBo-GFN and the classical GFN on real-world graphs with $C = 15$.

Distribution matching and loss We notice similar behaviors as with random graphs. Specifically, classical GFNs seem to be able to rival SubBo-GFN when C is small in terms of FCS, but it struggles to maintain this performance as C grows. SubBo-GFN-F still exhibits large confidence intervals, indicating a lot of variability in its FCS. A small loss once again translates to a small FCS for SubBo-GFN whereas the same cannot be said for other approaches when C is larger.

Top-100 Average Rewards When $C = 5$, SubBo-GFN and SubBo-GFN-F significantly outperform classical GFNs. However, there seems to be a trend of the classical GFN catching up to SubBo-GFN in terms of Top-100 Average Reward as C increases. Still, SubBo-GFN-F outperforms or rivals the classical GFN in Top-100 Average Reward. This indicates that leveraging bounds, specifically because they are numerous, seems to improve the discovery of high reward states.

Number of bounds We note that SubBo-GFN generates orders of magnitudes more training data than regular GFNs.

D. Implementation Details

We provide in Table 1 the parameters used for our experiments. For each batch of trajectories sampled with SubBo-GFN or the classical GFN are stored in a replay buffer. For SubBo-GFN, one epoch of training is done with the same batch size composed of a mix of trajectories generated from the upper bounds and from the replay buffer storing the sampled trajectories. We choose a mix of 25% from the replay buffer and 75% from trajectories sampled from the terminating states

for which we have upper bounds available. As there are usually many upper bounds for a single $x \in \mathcal{X}$, we select the smallest (tightest) before swapping it with R , to avoid artificially adding noise to the learning process. For training, classical GFNs operate similarly, but all of the trajectories used in training are from the replay buffer instead.

Table 1. Hyperparameter Configuration for GFN Graph Experiments

Category	Hyperparameter	Value
GFN Training	Learning Objective	Trajectory Balance (Malkin et al., 2022)
	Query Budget	10,000
	Batch Size (sampling and offline)	16
	Learning Rate (P_F, P_B)	10^{-4}
	Learning Rate (Z)	10^{-2}
Architecture	Model Type	Graph Isomorphism Network (Xu et al., 2018)
	Embedding Dimension	128
	Convolutional Layers	1
FCS	Forward Trajectories	128
	Backward Trajectories	8
	Epochs	25

Hardware Details We run all of our experiments on H100 NVIDIA GPUs. The CPUs for these experiments vary, as multiple clusters were used. CPUs were either AMD EPYC 9454, Intel Xeon Gold 6448Y, Intel Xeon Platinum 8570.